FACULTY OF TECHNOLOGY

FABRICATION OF WET SPUN CORE-SHELL FILAMENTS FROM FUNCTIONALIZED NANOCELLULOSES

Kaisa Juntunen

PROCESS ENGINEERING

Master's thesis

August 2021

ABSTRACT

Fabrication of Wet Spun Core-shell Filaments from Functionalized Nanocelluloses

Kaisa Juntunen

University of Oulu, Degree Programme of Process Engineering

Master's thesis 2021, 83 pp. + 3 Appendixes

Supervisors at the University: Ossi Laitinen and Terhi Suopajärvi

The aim of this thesis was to investigate a novel wet spinning process based on interfacial complexation of functionalized nanocelluloses for the production of core-shell filaments or yarns. The work focused on wet spinning process development, and investigated how winding and drying steps could be integrated in the continuous spinning process, in which interfacial complexation and wet spinning are combined for filament fabrication of oppositely charged cellulose nanofibers (CNF). Additionally, the effect of processing parameters such as drying temperature, spinning speed, needle size, washing and stretching on mechanical properties of the filaments were investigated to optimize the process.

A continuous process was developed by investigating different types of CNF core-shell combinations and by integrating separate unit operations to obtain a continuous filament fabrication. Three different types of filaments consisting of functionalized anionic-cationic or anionic-anionic CNF pairs (S-CNF/CDAC-CNF, TO-CNF/CDAC-CNF, and TO-CNF/TO-CNF) were successfully fabricated. The requirement for feasible continuous process and homogenous filament fabrication were the filament structure consisting of anionic core and cationic shell, proper air removal from CNFs, filament support and reduced friction during the processing, properly directed drying air and Teflon covered winder. In addition, drying temperature, spinning speed and needle size of the process were optimized. The structure of filaments were investigated by microscopy and mechanical properties were analyzed using tensile tests.

Stretching was shown to be an important parameter for better CNF orientation and improved mechanical properties. Additionally, washing stage significantly increased tensile strengths of the filaments. The highest tensile strength was reached with washed

S-CNF/CDAC-CNF, which was purely based on CNFs which were obtained through a green synthesis route in the deep eutectic solvent (DES). Overall, the results showed the technical feasibility of continuous process for fabrication of core-shell filaments based on functionalized nanocelluloses. However, further research is still needed to improve the CNF orientation and mechanical properties, and to develop the process by incorporating e.g. washing step.

Keywords: continuous spinning, filament, interfacial complexation, nanocellulose, textile fibers, wet spinning

TIIVISTELMÄ

Fabrication of Wet Spun Core-shell Filaments From Functionalized Nanocelluloses

Kaisa Juntunen

Oulun yliopisto, prosessitekniikan tutkinto-ohjelma

Diplomityö 2021, 83 s. + 3 liitettä

Työn ohjaajat yliopistolla: Ossi Laitinen ja Terhi Suopajärvi

Tämän diplomityön tarkoituksena oli tutkia uutta funktionalisoitujen nanoselluloosien rajapintakompleksointiin perustuvaa märkäkehruuprosessia ydin-kuori filamenttien tai lankojen valmistusta varten. Työ keskittyi märkäkehruuprosessin kehittämiseen ja työssä selvitettiin kuinka kelaus- ja kuivausvaiheet voisi yhdistää jatkuvatoimiseen prosessiin, jossa varaukseltaan vastakkaisista nanoselluloosista (CNF) valmistetaan filamentteja yhdistämällä rajapintakompleksointi ja märkäkehruu. Prosessin optimoimiseksi myös prosessiparametrien kuten kuivauslämpötilan, kehruunopeuden, neulan koon, pesun ja venytyksen vaikutuksia filamenttien mekaanisiin ominaisuuksiin tutkittiin.

Jatkuvatoiminen prosessi kehitettiin kokeilemalla filamenteille erilaisia CNF ydin-kuori -yhdistelmiä ja yksikköoperaatiot liitettiin toisiinsa jatkuvien filamenttien valmistamiseksi. Työssä valmistettiin onnistuneesti kolme koostumukseltaan erilaista filamenttia, jotka koostuivat funktionalisoiduista anioninen-kationinen tai anioninen-anioninen CNF-pareista (S-CNF/CDAC-CNF, TO-CNF/CDAC-CNF, ja TO-CNF/TO-CNF). Filamenttien rakenne, joka muodostui anionisesta ytimestä ja kationisesta kuoresta, ilman poistaminen CNF:stä, filamenttien tukeminen ja kitkan vähentäminen prosessin aikana, kuivausilman oikea suuntaaminen sekä kelaimen Teflon-pinta olivat edellytys jatkuvatoimisen prosessin ja homogeenisten filamenttien valmistamisen kannalta. Lisäksi prosessin kehruunopeus, kuivauslämpötila ja neulan koko optimoitiin. Filamenttien rakennetta tutkittiin mikroskopialla ja lujuusmittausten avulla selvitettiin filamenttien mekaanisia ominaisuuksia.

Venytyksen osoitettiin olevan tärkeä parametri CNF:n paremman orientaation ja mekaanisten ominaisuuksien kannalta. Lisäksi filamenttien peseminen paransi niiden vetolujuuksia. Paras vetolujuus saatiin pestylle S-CNF/CDAC-CNF filamentille, joka

valmistettiin käyttämällä vihreitä syväeutektisia liuottimia (DES). Kaiken kaikkiaan tulokset osoittivat ydin-kuori filamenttien jatkuvatoimisen valmistuksen funktionalisoiduista nanoselluloosista olevan teknisesti mahdollista. Lisätutkimuksia kuitenkin tarvitaan CNF:n orientaation ja mekaanisten ominaisuuksien parantamiseksi sekä prosessin kehittämiseksi, esimerkiksi liittämällä pesuvaihe prosessiin.

Asiasanat: jatkuvatoiminen kehrääminen, filamentti, rajapintakompleksointi, nanoselluloosa, tekstiilikuidut, märkäkehräys

PREFACE

The purpose of this thesis was to investigate a wet spinning process based on interfacial complexation of functionalized nanocelluloses for the production of core-shell filaments. The work was carried out for Fibre and Particle Engineering Research Unit of University of Oulu between January and August 2021.

I want to thank my supervisors, Ossi Laitinen and Terhi Suopajärvi, for their instructions and advices, and also Henrikki Liimatainen for discussions with you and your comments throught this project. Also, I want to show gratitude for the whole staff of the Fibre and Particle Engineering Research Unit, especially laboratory technicians Jani Österlund, Elisa Wirkkala and Jarno Karvonen for their help in the laboratory during my experimental part of the thesis.

Finally, I want to thank my family and friends for their support throughout my studies and this thesis.

Oulu, 31.8.2021

Kaisa Juntunen
Kaisa Juntunen

TABLE OF CONTENT

ABBREVIATIONS

AGU	anhydroglucose unit
CDAC-CNF	cationic dialdehyde cellulose nanofiber
CNC	cellulose nanocrystal
CNF	cellulose nanofiber
CSF	core-shell filament
DAC	dialdehyde cellulose
DES	deep eutectic solvent
DI	deionized
DP	degree of polymerization
DR	drawing ratio
HBA	hydrogen bond acceptor
HBD	hydrogen bond donor
INC	interfacial nanoparticle complexation
PEC	polyelectrolyte complec
SC-CNF	succinylated cellulose nanofiber
S-CNF	sulfonated cellulose nanofiber
TEMPO	2,2,6,6-tetramethylpiperidine-1-oxyl radical
TO-CNF	TEMPO-oxidized cellulose nanofiber

INTRODUCTION

Cellulosic fibers are essential in society since they are used in many everyday commodities such as textiles and papermaking, and they have considered to be one of the most potential raw materials for the emerging bioeconomy to create novel materials and applications for replacing non-renewable resources. However, one key challenge for wider use of cellulose is its recalcitrant and strong hydrogen bonded structure which make it difficult to tailor and modify cellulose. Cellulosic fibers have a natural hierarchical structure consisting of nanoscale entities. These nano-sized constituents, i.e. nanocelluloses, possess many unique properties being renewable and biodegradable and are one potential option for sustainable development and expanding applications of cellulose. Especially, bottom-up assembly of nanocellulose to hierarchical structures is a promising approach to produce various applications to replace plastic, glass and metal. (Ingrao et al. 2016; Jiang et al. 2018; Kumar et al. 2020; Nechyporchuk et al. 2019)

Recently, nanocelluloses have gathered grown interest as a building block for production of filaments or textile type yarns, as they can be shaped to strong, stiff and highly ordered continuous fibers, which could be environmentally friendly alternative for producing textiles, bio-composites and electronics. (Nechyporchuk et al. 2019, Marais et al. 2020) Previously continuous nanocellulose based filaments have been produced in laboratory scale using traditional wet spinning and flow focusing methods (Lundahl et al. 2018, Nechyporchuk et al. 2019). Zhang and Liimatainen (2018) successfully fabricated hierarchical filaments by using oppositely charged nanocelluloses via the method called interfacial complexation. In this work, wet spinning and interfacial complexation are combined to develop continuous filament fabrication process. Especially, following research questions were considered:

- How the filaments can be produced in a continuous process based solely on cellulose nanofibers?
- How drying and winding steps can be integrated in the production process to produce homogenous filaments?
- How different process parameters are affecting the physical properties of filaments?

The literature review of this thesis focuses on nanocelluloses and their continuous filaments. In the section related to nanocellulose, structure of cellulose as well as nanocellulose as a concept, its production methods and pretreatments, especially deep eutectic solvents (DES), are introduced. In the section of filaments, background of cellulosic filaments, their spinning methods, and various parameters attributed to spinning process are discussed.

The main target of the experimental part was to study and develop a continuous process for fabrication of core-shell filaments based on nanocelluloses through a combined wet spinning and interfacial complexation. Earlier the researchers in the Fiber and Particle Engineering Research unit studied a novel approach for the filament fabrication using interfacial complexation of oppositely charged nanocelluloses, but there was not a continuous process for the filament production. In the current work, a continuous fabrication process was developed by integrating core-shell fiber spinning, drying and winding steps to the process. Additionally, the process was optimized by means of drying temperature, spinning speed, washing, and needle size. Also, the effect of stretching on filament characteristics was studied. Mechanical properties of filaments were investigated by tensile tests to evaluate best available processing conditions.

1 NANOCELLULOSE

Cellulose is the most abundant biopolymer on Earth as it is one of the main components of nearly all the plants. For thousands of years, cellulose, as in the form of wood, cotton and other plant fibers, have been used as an energy source, building material and clothing. Attractive structure and properties, such as biodegradability, renewability, high strength, non-toxicity and chemical modifying capacity of cellulose, make it interesting green material for replacing fossil-based materials and to create more sustainable economy and environment. Currently, wood pulp is the most important raw material source for cellulose processing. Cellulose is mainly used for the production of paper and board, but also for production of regenerated cellulose such as synthetic fibers, films and membranes, and cellulose derivatives, which are used in various applications such as coatings, pharmaceuticals and cosmetics. (Klemm et al. 2005; Dufresne 2018 p. 621)

Nanostructured cellulose materials were introduced already in the 1940s when cellulose nanocrystals (CNC) were found and later in the 1980s in the form of microfibrillated cellulose (MFC). Nowadays, nanocelluloses have been revealed and developed in a wide range of applications. Mechanical, rheological, optical and film-forming properties of nanocellulose make it fascinating material for many novel purposes such as composites, food applications, packaging, coatings, adhesives, filtration and materials in electronics and biomedicine. (Dufresne 2018 p. 621-624)

Currently novel applications of cellulose are searched for intensively. More environmentally friendly alternatives to petroleum and product derived from it are required to support the general sustainability targets. Abundant and renewable plant resources are apparent responses for this demand. Therefore, nanocelluloses have increased attention because of their unique properties and innovative applications offer promising replacements for fossil-based products, such as plastics and packaging applications. (Klemm et al. 2011; Dufresne 2018 p. 622; Kalia et al. p.150).

1.1 Cellulose

Cellulose is a linear unbranched carbohydrate polymer consisting of β-D-glucopyranose, also called anhydroglucose units (AGU), which are connected via β-glycosidic bonds

between C1 and C4 carbon atoms. Every second AGU ring is rotated 180° towards each other, to form a repeating unit of cellulose, i.e. cellobiose, as shown in Figure 1. The chain length of cellulose, the degree of polymerization (DP), is determined by the number of AGUs. It varies with the origin and treatment of the raw material. DP values of over 10 000 are reported for some native celluloses, being one of the longest polysaccharides. DP value is typically 250-500 for regenerated cellulose, and 800-1000 for cotton. (Ek et al. 2009, p. 89-90; Klemm et al. 2005)

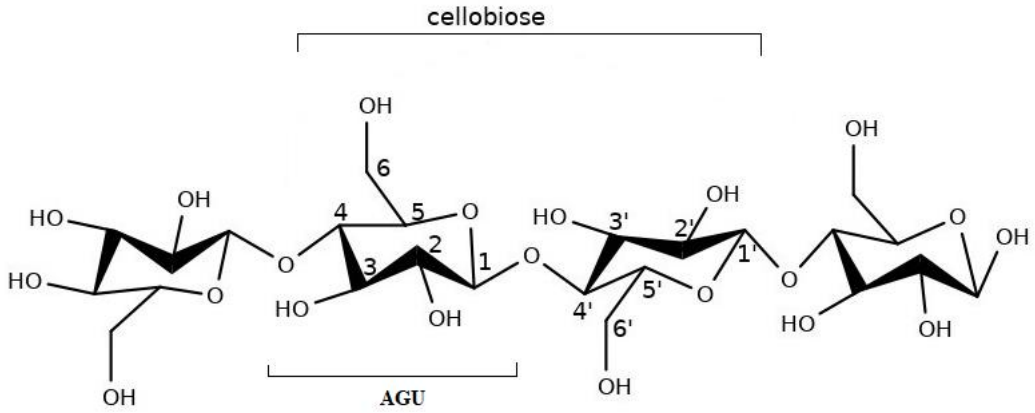

Figure 1. Molecular structure of cellulose (retelling Ek et al. 2009, p. 90).

Each monomer of cellulose bears three hydroxyl groups. Their hydrogen bonding ability play a major role in directing crystalline packing and determining physical properties of cellulose. (Dufresne 2018, p. 5) The hydrogen bond network gives the cellulose chains a high axial stiffness and makes cellulose a stable polymer, that does not dissolve in typical solvents (Eichhorn et al. 2010). Cellulose polymeric chains have reducing and nonreducing ends. The reducing end is terminated with an original C1-OH group, and the nonreducing end is terminated with D-glucose unit with an original C4-OH group. The molecular structure of cellulose provides its characteristic properties such as hydrophilicity, chirality, degradability and high chemical variability commenced by the donor reactivity of the OH groups. (Klemm et al. 2005)

Cellulose has several polymorphs, due to its crystalline structure. Hydroxyl groups and oxygen atoms in cellobiose offer many possibilities of various hydrogen bonding systems. Thus, cellulose exist in numerous crystal packings. In nature cellulose is discovered in the crystalline form of cellulose I, native cellulose. Cellulose I is composed of more than

one crystalline form and is a mixture consisting of two polymorphs; cellulose Iα and Iβ. Native cellulose can be transformed irreversibly into the thermodynamically more stable cellulose II by regeneration or mercerization. (Dufresne 2018, p. 8-10) Cellulose II differs from cellulose I so that the chains are antiparallel, following one more hydrogen bond per glucose residue in cellulose II. (Ek et al. 2009, p. 93) There are also cellulose III and IV of which cellulose I can chemically be converted to, but their structures are less important (Dufresne 2018, p. 93).

1.1.1 Hierarchical structure of cellulose

The presence of hydroxyl groups along the cellulose chains produces a network of intra- and intermolecular hydrogen bonds. Furthermore, van der Waals connections are formed between the chain layers. This ordered molecular alignment of cellulose chains parallel to each other is the base of an elementary fibril (i.e. nanofibril) (Ciolacu and Popa 2010, p. 9) with a typical diameter of 3-5 nm (Klemm et al. 2011). These elementary fibrils are packed into a bundles, called microfibrils, together with hemicellulose and lignin. Hierarchical structure of lignocellulosic fibril is presented in Figure 2. Microfibril is a slim (diameter of 10-30 nm), rod-like entity, which forms the basic structural unit of the plant cell wall. Microfibril have a length of several hundred nm and contain both crystalline and amorphous regions. (Dufresne 2018, p. 11-12,15; Klemm et al. 2011; Ciolacu and Popa 2010)

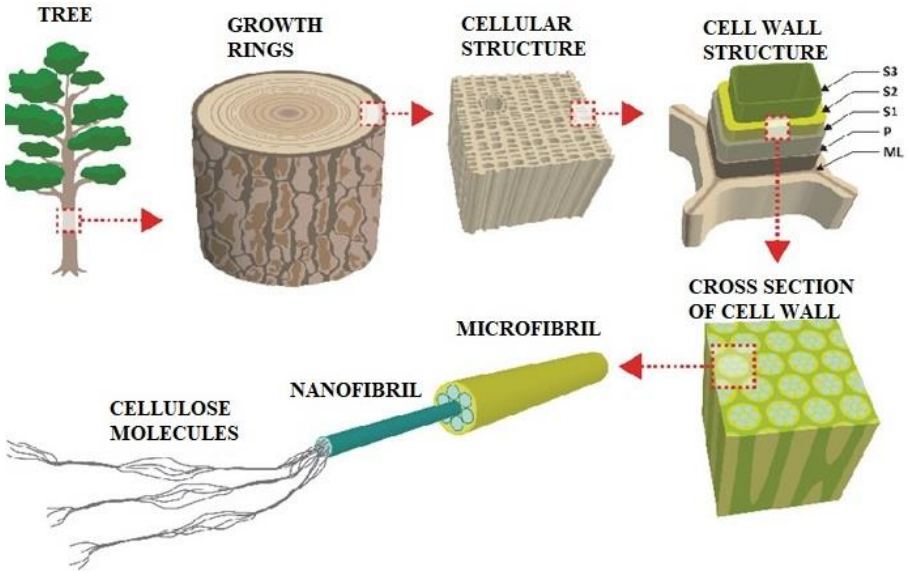

Figure 2. Hierarchical structure of lignocellulosic fiber (retelling Kekäläinen 2016, p. 21).

1.1.2 Fibre wall structure

Microfibrils aggregate together forming cell wall (Dufresne 2018). Basically, the plant cell wall is composed of two layers; primary wall (P) and secondary wall (S). Based on microfibrillar orientation, the secondary wall is divided into three sublayers: the outer layer (S1), the middle layer (S2), and the inner layer (S3) of secondary wall. Between the P walls of adjacent cells is middle lamella (ML). Centre of hollow fiber is lumen (L). Cell wall structure is presented in Figure 3. Secondary wall layers differ from each other based on orientation of their structural elements and chemical composition. (Stenius 2000, p. 25) Microfibrils orient differently in different layers of the cell wall, that have an influence on the physical properties of a wood fibers. Primary wall is a thin (0.05-0.1 µm) wall, where microfibrils are randomly arranged. In the secondary wall microfibrils are arranged in a spiral shape. Thickness of the S1-layer is 0.1-0.3 µm and there is 3-6 microfibrillar layers that are arranged in a left- and right-hand spiral with a pitch to the vertical axis of 50-70°. S2-layer is thickest of the layers (1-8 µm). There are 30-150 microfibrillar layers with a pitch of 5-30° to the vertical. Thin S3-layer have under 6 microfibrillar layers with a pitch of 60-90° to the vertical. (Stenius 2000, p. 25; Dinwoodie 1978) S2 is mostly responsible for the physical properties of a wood fiber because S2-layer increases with an increase in wall thickness, while thickness of S1- and S3-layers are constant. The relative mass proportion of cellulose is also highest in the S2-layer. (Stenius 2000, p. 24, 26, 33).

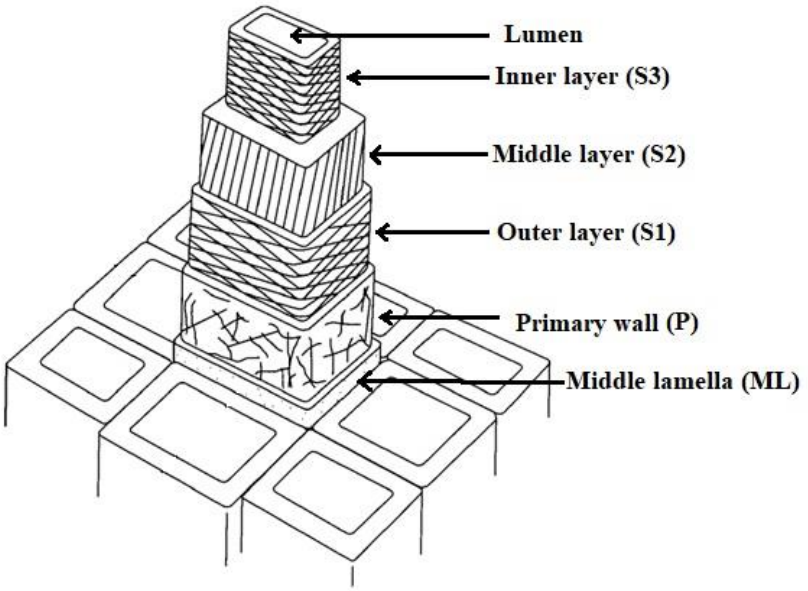

Figure 3. Cell wall structure (retelling Dinwoodie 1978).

Besides cellulose, other major chemical components of all wood species and most of the other lignocellulosic raw materials are hemicellulose and lignin, which together determine properties of wood or lignocellulose. Hemicellulose is carbohydrate building up from various sugar units; hexoses and pentoses. Compared to cellulose, hemicellulose has lower chemical and thermal stability, due to lower degree of DP ~150-200. (Christopher 2012) Lignin is a complex and amorphous aromatic polymer, which chemical structure is not exactly known. It differs from cellulose and hemicellulose by low degree of order and high degree of heterogeneity in structure. Lignin acts as binder between wood cells and gives the rigidity to the cell wall and resistance to degradation. (Dhillon et al. 2012 p. 3; Gargulak et al. 2015)

Content of the components vary between softwood and hardwood. Average cellulose content is 40-45% of the wood dry solids. Hemicellulose content of the dry wood solids is 30-35% and lignin content 25-30%. There are also small quantities, less than 5%, of other components such as extractives, pectin, starch, proteins, water-soluble organics, and inorganics in wood. (Stenius 2000, p. 28)

1.2 Nanocellulose

Nanocellulose refers to cellulose particles, that have at least one dimension in nanoscale (1-100 nm). Wood, deciduous plants, and agricultural by-products e.g. cotton, flax, hemp, sugan cane and wheat stalk may be used as a raw material for nanocellulose, while wood pulp being the most important raw material for nanocellulose isolation. (Kangas 2014, p.8-9; Stelte and Sanadi 2009).

Based on production method, dimensions, and characteristics, nanocellulose can be divided into two major nano-scale classes: cellulose nanofibrers (CNF) and cellulose nanocrystals (CNC), which are produced from cellulose fibers by disintegration (top-down process). Also, bacterial cellulose (BC) and electrospun cellulose nanofibers (ECNF) are considered as nanocellulose. They are produced from low molecular weight sugars by bacteria or from dissolved cellulose by electrospinning (bottom-up processes). (Nechyporchuk et al. 2016)

Nanocelluloses combine many appealing cellulose properties such as hydrophilicity, chemical modification capacity and formation of adaptable fiber morphologies with the properties of nano-scale materials such as reactivity and bonding capability caused by the large surface area of nano-sized materials (Kangas 2014 p. 8). Nanocelluloses have wide range of applications such as composites, strengthening agent for paper and board, coatings, packaging, food industry, adhesives, printing, electronics, energy storage applications, sensors, emulsions, filtration, cosmetics, and biomedical applications. (Dufresne 2019) One novel promising area is continuous filament structures. These filaments are the basic raw material for many applications such as composites and textile applications. (Ghasemi et al. 2018)

1.2.1 Cellulose nanocrystals (CNC)

Cellulose nanocrystals are rod-like and rigid particles produced typically using mineral acid hydrolysis, that disintegrates and dissolves amorphous regions of cellulose while crystalline regions of cellulose remain unbroken. Typically, CNCs have a diameter of 3-35 nm and a length of 200-500 nm. (Nechyporchuk et al. 2016) Sulfuric acid, hydrochloride acid, hydrobromide acid and phosphoric acid are commonly used for CNC production. These strong acids generate CNCs with high crystallinity. CNCs can also be extracted using weak carboxylic acids such as acetic acid and lactic acid. However, weak acids results into more fibrous morphology and lower crystallinity. Thus, weak acid hydrolysis is often combined with mechanical disintegration to improve the quality of CNCs. (Dhali et al. 2021) Terminology regarding to CNC has been wide. In addition to cellulose nanocrystal, nanocrystalline cellulose, whiskers and crystallites have been used (Klemm et al. 2011).

1.2.2 Cellulose nanofibers (CNF)

Cellulose fibers can be disintegrated into its substructural nano-scale units, nanofibers, to produce nanofibrillated cellulose or cellulose nanofibers or nanofibrils (Habibi 2014). Nanofibers are long and flexible, containing both crystalline and amorphous regions of cellulose (Tingaut et al. 2012). Commonly CNFs are produced via intensive mechanical disintegration, which cuts hydrogen bonds between the fibers. Source of cellulose and production process influence the diameter distribution of CNF that is usually between 5-50 nm while length varies from hundreds of nanometers to few micrometers.

(Nechyporchuk et al. 2016) Microfibrillated cellulose (MFC) is another term used to refer elongated and flexible nano-sized constituents of celluloses. However, MFC consist typically larger nanofiber aggregates, and has a less uniform size distribution. (Dufresne 2019).

1.3 Production of cellulose nanofibers

Generally cellulose CNF is produced with mechanical methods, that utilize shear forces to nanofibrillate cellulose (Nechyporchuk et al. 2016). However, pure mechanical methods consume a lot of energy, damage the microfibril structure or fail to disintegrate the pulp enough. Thus, cellulose pretreatments are usually necessary to obtain high quality, individualized CNFs and enhance the production process (Dufresne 2019, Henriksson et al. 2007). By combining chemical or enzyme pretreatments with mechanical treatment, it is possible to reduce energy consumption from 20 000 – 30 000 kWh/ton to the level of 1 000 kWh/ton. (Siró and Plackett 2010).

1.3.1 Mechanical disintegration

The purpose of mechanical disintegration is to separate the nanofibers by inducing strong shear forces in the interfibrous hydrogen bonded CNF network. CNFs are generally produced in aqueous medium, and cellulose is dispersed at low concentrations, below 5 wt%, to prevent reverse association of separated nanofibers and loosen the hydrogen bonding between them. Typical mechanical methods for CNF production are homogenization, microfluidization and grinding. These are the most efficient techniques for delamination of fiber cell wall and CNF isolation, also currently used for industrial scale production of CNF. There are also non-conventional methods such as cryo-crushing, ultrasonication, extrusion, steam explosion, ball milling, aqueous counter collision, blending, and refining. (Nechyporchuk et al. 2016)

High pressure homogenization is a commonly used method, which can utilize both homogenizers and microfluidizers. The principle of microfluidizer involves passing the cellulose suspension at high pressure through a thin (diameter of 100-400 μm) chamber with Z- or Y-shape. Strong shear forces and collision of cellulose suspension against the walls yields the cellulose nanofibrillation. (Nechyporchuk et al. 2016) This technique has successfully been utilized to produce CNF in many previous studies e.g. Pääkkö et al.

(2007) and Naderi et al. (2015). High energy consumption and clogging of the microfluidizers have been noticed to be the main disadvantages for commercial favour of homogenization. Clogging is connected to the aggregation of fibers. In avoiding clogging, the modification of surface charge density of fibers is an efficient approach. (Lindström 2017)

1.3.2 Pretreatments

Since mechanical disintegration of cellulose is highly energy consuming, cellulose pretreatment is often necessary (Dufresne 2019). There are numerous methods to obtain less stiff and cohesive fibers, therefore reducing the energy needed for nanofibrillation. Predominantly, three alternatives that can be used together or separately for pretreatment are (1) limiting the hydrogen bonding in the cellulose, (2) adding a repulsive charge, and (3) reducing the DP or the amorphous connection between individual nanofibers. (Dufresne 2019) Biological and chemical pretreatments both have shown to enhance nanofibrillation and reduce energy demand. Pretreatments also strongly affect the properties of resulting CNF. (Nechyporchuk et al. 2016)

Moreover, enzymatic hydrolysis has shown to be effective pretreatment for CNF preparation. Enzymes, as cellulase, facilitate disintegration of cellulosic pulp into nanofibers by catalysing the hydrolysis of cellulose thus improving cellulose nanofibrillation. (Pääkkö et al 2007, Henriksson et al. 2007) Chemical modification of cellulose by endowing cationic and anionic groups on the surface of cellulose nanofibers promotes the nanofibrillation due to electrostatic repulsion between ions at the surface of the nanofibers, thus preventing formation of hydrogen bonds (Nechypochuk et al 2016; Saito et al. 2007). One of the most common pretreatments is 2,2,6,6-tetramethylpiperidine-1-oxyl radical (i.e. TEMPO)-mediated oxidation, which have successfully used to obtain individualized cellulose nanofibers. TEMPO-mediated oxidation regioselectively converts the C6 primary hydroxyl groups of cellulose to anionic C6 carboxylate groups. (Dufresne 2019; Saito et al. 2007) Periodate-chlorite oxidation (Liimatainen et al. 2012), sulfonation (Liimatainen et al. 2013), carboxymethylation (Wågberg et al. 2008) are other methods introduce negatively charged groups on the surface of cellulose nanofibers. Cationization by quaternization have been reported as an effective pretreatment for CNF production (Olszewska et al. 2011). The charge content of native wood is very low but increase during cellulose

impregnation, pulping and bleaching, in which case the charge content varies between 20 and 300 μeq/g. Chemical modification of cellulose increase the charge content to the range from 300 to 2000 μeq/g. (Lindström 2017)

1.3.3 Deep eutectic solvents (DES)

Deep eutectic solvents (DESs) are relatively novel chemicals used as a pretreatment for nanofibrillation of cellulose. DESs are environmentally friendly solvents, which can offer sustainable way producing CNFs without intensive mechanical and chemical modification of cellulose. (Sirviö et al. 2015)

Abbot et al. (2003) first presented the idea of deep eutectic solvent as a new type of ionic liquid. Interaction of solid quaternary ammonium salts (e.g. choline chloride) with hydrogen bond donor (urea) could form eutectic mixture that have melting point lower than either of the component. In case of choline chloride/urea, melting point of the eutectic mixture is 12 °C, which is lower than melting point of choline chloride (302 °C) and urea (133 °C).

The most reported DESs are formed by mixing a quaternary ammonium salt with a hydrogen bond donor (HBD), typically an alcohol or amide (urea, glycerol or ethylene glycol). Choline chloride (ChCl) is one of the most used hydrogen bond acceptor (HBA) for DES production. 1:2 molar ratio mixture of choline chloride and urea is the most studied DES. (Zhang et al. 2012; Smith et al. 2014)

There are various theories to explain the eutectic phenomena. Early studies indicated decrease in the melting point in DESs is due to the charge delocalization occurring through hydrogen bonding between the halide anion and the HBD. (Carriazo et al. 2012) Recently, this mechanism has been challenged. Negligible charge transfer from chloride to urea in ChCl/urea DES is occurring, disclaiming charge delocalization (Zahn et al. 2016) Also, diverse variety of hydrogen bonds, neutral, ionic and doubly ionic, exhibit within ChCl-urea DES. It is recognized that urea acts as both HBD and HBA, thus forming an anionic complex with chloride or cationic complex with choline. Thus, the charge distribution within these groups is merged by urea, not of a complex with delocalised charge. (Ashworth et al. 2016) Regardless, a well-defined hydrogen bond

network between urea-urea, and urea-ChCl are balanced leading to a strong intercalation of HBD into a salt network, thus decreasing melting point (Stefanovic et al. 2017).

DESs can be classified into four groups depending on the nature of the complexing agent. Type I DESs are systems comprising of metal halide and imidazolium salt. Type II are formed between hydrated metal halides and quaternary ammonium salt. Previously mentioned ChCl-urea DES is included to type III, which are the most common DESs. They are formed by mixing quaternary ammonium salt with a HBD, such as urea, glycerol or ethylene glycol. (Smith et al. 2014) Type IV are formed between metal salts, such as $ZnCl_2$, and organic alcohols or amides (Abbot et al. 2007). A new set of DESs, so called natural deep eutectic solvents (NADES) have also been discovered (Choi et al. 2011). NADES are mixtures composed of primary metabolites, such as sugars, sugar alcohols, amino acids, organic acids, and choline derivatives (Dai et al. 2013).

Usually, DESs are cheap, nontoxic, biodegradable and easy to prepare, since it involves just mixing and mild heating of two components (Smith et al. 2014). These properties make DESs potential green solvents, reagents or catalysts for many applications such as CO_2 and metal oxide dissolution, biodiesel purification and in synthesis of cellulose derivatives (Zhang et al. 2012)

Sirviö et al. (2015) first used DES as a pretreatment for the nanofibrillation of wood cellulose. DES based on choline chloride-urea (molar ratio of 1:2) was shown to be mild pretreatment media. DES penetrated cellulose thus breaking hydrogen bonding. It has been indicated that cationic choline ions are interacting with the anionic groups of cellulose fibers through electrostatic interaction (Tenhunen et al. 2018). DP value of cellulose remained at the same level as the initial cellulose, thus no dissolution of cellulose occurred during treatment. Besides crystallinity of cellulose remained the same after treatment as before it. (Sirviö et al. 2015)

Anionic groups on the surface of the cellulose have been created using e.g. succinylation with urea-LiCl DES (Selkälä et al. 2016) and sulfation with sulfamic acid-urea DES (Sirviö et al. 2019). Also DES based on imidazole and TEMACI has been found to be an effective reaction medium for carboxymethylation of wood cellulose (Sirviö and Visanko 2017). The introduction of cationic groups on cellulose fibers using DES have also been demonstrated. DES, based on triethylmethylammonium chloride (TEMA) and imidazole,

have been used as a reaction medium for cationization of cellulose. Trimethylglycine (betaine) hydrochloride was used as a cationization reagent and p-toluenesulfonyl (tosyl) chloride as a coupling agent in the reaction between the cellulose and betaine. (Sirviö 2018) In addition, DES based on aminoguanidine hydrochloride and glycerol (AhG) have been used to cationize celluloses. Cellulose was first oxidized to dialdehyde cellulose (DAC) using sodium periodate, following cationization by AhG DES. (Li et al. 2018)

2 CELLULOSIC FILAMENTS

Generally different textile fibers or continuous filaments are classified into two categories; natural and man-made fibers. Natural fibers include fibers based on vegetables and animals such as cotton, flax, hemp and wool. Man-made fibers are fabricated from either synthetic polymer (fossil-based resources) or natural polymers. Natural polymers, such as cellulose, can be converted into viscose, modal and lyocell, for example. In the end of 19th century, industrial fabrication of artificial fibers begun. Nitrated form of cellulose was dissolved in alcohol and ether following filament drawn into the air. Subsequently cupro, viscose and lyocell processed were pioneered. Principle of all these processes is first dissolve cellulose and then precipitate it in coagulation bath. (Woodings 2001, p. 2-18)

During precipitation and following drying of cellulose fibers, cellulose I is transformed into cellulose II, which have lower elastic modulus due the loss of intermolecular hydrogen bonds. Thus natural cellulose fibers have better mechanical properties than regenerated fibers. Consequently, instead of dissolution, possible development in fiber fabrication could be filament spinning from nanocellulose, which can maintain the cellulose I structure. (Iwamoto et al. 2011)

2.1 Nanocellulose based filaments

Spinning of continuous fibers from nanocellulose is fascinating due to fact that nanocellulose has many unique properties and it still maintains cellulose I structure. Nanocellulose based continuous fibers or filaments can be prepared using solely nanocellulose suspensions or a combination of nanocellulose with natural or synthetic polymers. (Fahma et al. 2020) In addition, CNF based filaments can be produced without the need for cellulose dissolution and regeneration (Lundahl et al. 2017). They can also be more sustainable option than traditional regenerated celluloses, which need organic toxic chemicals and solvents (Håkansson et al. 2014).

Earlier studies have indicated that CNF filaments can have the strength similar to the strongest commercially available regenerated cellulose filaments. Therefore, nanocellulose based filaments can enable development of textile products in near future, which could replace cotton, viscose and Lyocell, and offer green alternative materials for

other applications such as high-performance bio-composites, biomedical applications (Mertaniemi et al. 2016) and electronic devices (Marais et al. 2020). (Håkansson et al. 2014)

2.2 Spinning methods for nanocellulose based filaments

Cellulosic filaments can be produced by several spinning methods; dry spinning, wet spinning, dry-jet wet spinning, melt spinning and electrospinning. Wet and dry spinning are the only techniques that can be used directly for CNF hydrogels without added polymers. (Lundahl et al 2017) As the CNF are widely available in the form of aqueous hydrogels, nanocellulose filaments have been produced mainly by wet spinning using syringe extrusion, flow focusing and coaxial spinning (Rosén et al. 2020). Additionally, interfacial complexation of oppositely charged cellulose nanofibers has been reported to lead organized structure and exceptional mechanical properties (Grande et al. 2017).

2.2.1 Traditional wet spinning

Wet spinning is the oldest known process for spinning of man-made fibers. Filaments are produced by extruding a polymer solution through a spinneret into a coagulation bath as shown in the Figure 4. (Rosén et al. 2020) Iwamoto et al. (2011) first prepared continuous fibers from cellulose nanofibers. Cellulose nanofibers were obtained by TEMPO-mediated oxidation (TO-CNF) from wood cellulose. Dispersion of TO-CNF at 1 wt% concentration was ejected through a syringe needle into a coagulation bath. Filaments had smooth surfaces and hollow structure at high spinning rate. Using the wet spinning technique of TO-CNF, filaments with tensile strength of 297 MPa and Young's modulus of 21 GPa were achieved (Lundahl et al. 2016).

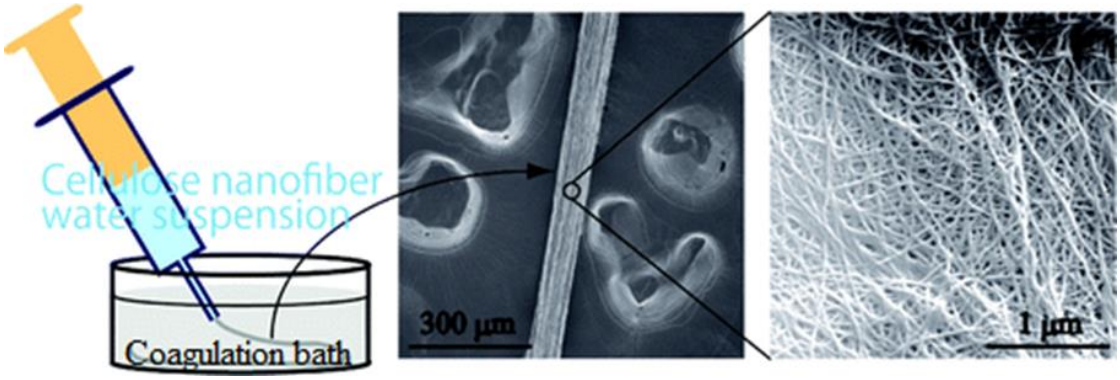

Figure 4. The principle of traditional wet spinning (retelling Iwamoto et al. 2011).

2.2.2 Wet spinning by flow focusing

Alignment of nanocellulose in the filament is a key factor in its mechanical properties. For better alignment, flow focusing was applied for filament wet spinning to control the assembly of CNFs. In this concept CNF dispersion is first aligned followed by gelation. Flow-assisted assembly is usually performed using double-sheath flow focusing device, in which CNF suspension is injected in the core flow, deionized (DI) water in the first sheath flow, and acid at low pH in the second sheath flow. Figure 5 demonstrates the principle of double-sheath flow focusing system. In the core flow, CNFs are free to spin due the electrostatic repulsion between nanofibers. The first sheath flow, aligns the nanofibers toward the flow direction. It also supports electrostatic repulsion between CNF. Before losing the alignment due to Brownian diffusion, electrostatic repulsion between the CNF is diminished by an electrolyte diffusion using second flow. This withdraw of the electrostatic repulsion leads to gelation i.e. coagulation of CNF. Second flow also improves the nanofiber alignment. For additional gelation, suspension can be extruded into the coagulation bath with same pH as in the second sheath flow (Nechyporchuk et al. 2019). Unidirectional alignment of CNF into fibers is gained using this method. Produced filaments have shown to be as strong as strongest commercial cellulose filament, but also stronger and stiffer than traditionally wet spun continuous fibers. (Håkansson et al. 2014; Mittal et al. 2018)

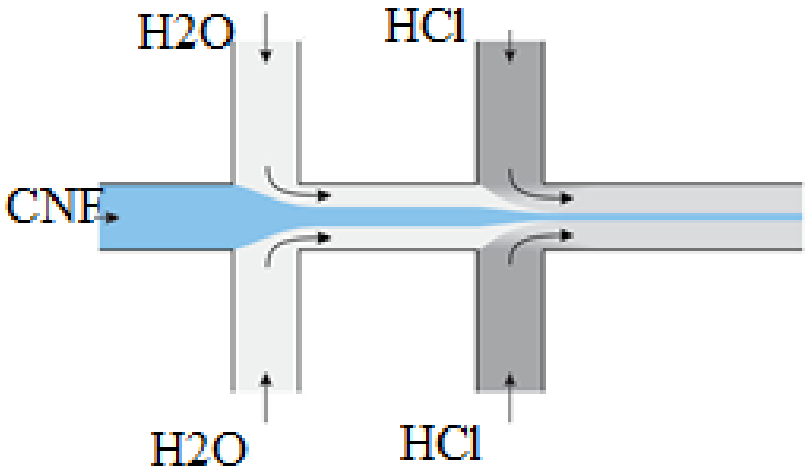

Figure 5. Double-sheath flow focusing system (retelling Nechyporchuk et al. 2019).

Both CNC and CNF have been used in the core flow, but strongest filaments have been produced using CNF because of their much higher length. Based on flow focusing,

filaments with better mechanical properties compared to traditional wet spun filaments were fabricated. Using TO-CNF, tensile strength of 1.57GPa and Young's modulus of 86 GPa was achieved. (Mittal et al. 2018)

2.2.3 Coaxial spinning

Previously CNF filaments based on core-shell structure were produced using a wet spinning process with two syringes connected to a coaxial needle. To produce these core-shell filaments (CSF) coaxial needle mounted with an extension tube is used to allow filament preparation through flow acceleration, CNF orientation and self-association steps similar to wet spinning using flow-focusing. (Marais et al. 2020) Coaxial wet spinning provide utilizing core material that is not spinnable on its own by enclosing it inside a protective shell. Continuous CSFs have also been produced using method called dry-jet wet spinning with coaxial spinning (Reyes et al. 2020), in which spinning dope is extruded into coagulation bath through an air gap, which allows drawing, thus additional orientation of nanofibers. (Figure 6).

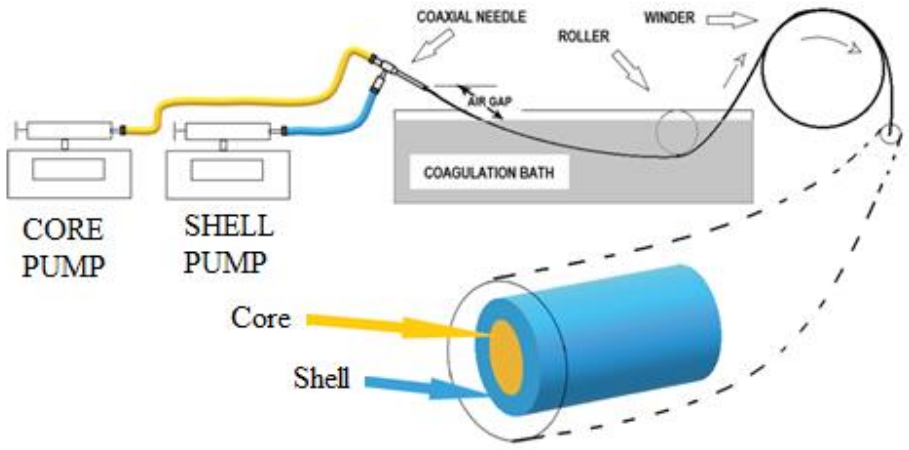

Figure 6. Coaxial spinning (retelling Reyes et al. 2020).

Earlier coaxial spinning has been performed using CNF dispersion in the core with the shell composing of cellulose solution in ionic liquid (Reyes et al. 2020), guar gum, cellulose acetate (Lundahl et al. 2018) and carbon nanotubes (Marais et al. 2020). Lundahl et al. (2018) discovered that core-shell structure was essential for the continuous formation of filaments at high spinning speeds, as the filaments broke in the absence of a shell. Cellulose acetate and guar gum were effective supporting polymer as a shell

material allowing control of filament properties. Core and shell interacted between each other, and it was detected that limited orientation of fibers could be compensated by a strong interfacial affinity between the components of core and shell.

Similar results were discovered by Reyes et al. (2020), that used TO-CNF as a core with protic ionic liquid (PIL) as a shell. Strong interfacial adhesion between core and shell was observed. Core-shell filaments had a smooth surface and regular cylindrical shape, while filaments composed of TO-CNF core without shell had irregular surface and poor CNF alignment, which was appeared as flocculated nanofibers in the filaments. CSFs were also more flexible, less brittle and elongation rose from 2 to 18% compared to the TO-CNF filaments.

2.2.4 Interfacial complexation spinning

Complexation of oppositely charged nanocelluloses and other molecules have a positive impact on alignment of constituents during spinning and thus on mechanical properties of filaments. Continuous CNF filaments have been created between anionic TO-CNF and cationic chitosan. Ionic association between the interface of oppositely charged nanocellulose and biopolymer produced stiff and flexible filaments with compact structure and good alignment of CNF in the drawing direction. (Grande et al. 2017)

Recently, it was found out that a system consisting only of oppositely charged nanoparticles could also form filaments. A novel phenomenon, referred as interfacial nanoparticle complexation (INC), resulted in the complexation of oppositely charged cellulose nanoparticles. Cationic cellulose nanocrystals with anionic celluloses in aqueous suspension were applied to fabricate hierarchical filaments. Filaments were produced via simple method: two oppositely charged nanocellulose droplets were placed adjacent to each other and made into contact. Ionic interaction between oppositely charged nanocelluloses formed nanosized subunit nanofibers, which bonded together forming filaments within packing in parallel as interface film was picked up and drawn vertically. Highest mechanical properties in terms of tensile strength (153 MPa) and Young's modulus (8.4 GPa) were gained with complexation of cationic cellulose nanocrystals and TO-CNF. (Zhang and Liimatainen 2018) Similarly, cationic CNC with anionic graphene oxide (Zhang et al. 2020a), and anionic TO-CNF with cationic chitin

nanocrystals (Zhang et al. 2020b) have been used to produce continuous filaments using INC.

Using INC spinning, mainly side-by-side filaments have been produced, which enable only discontinuous filament processes. Recently interfacial complexation based on a core-shell spinneret was introduced for continuous production of filaments. Polyelectrolyte complex (PEC) fibers as a core-shell structure were produced using a spinneret as shown in Figure 7. (Cui et al. 2020)

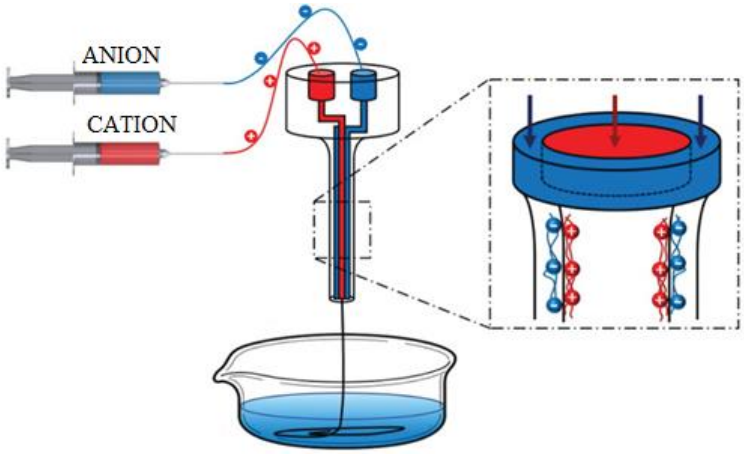

Figure 7. Interfacial complexation within a spinneret (retelling Cui et al. 2020).

Combination of flow focusing and interfacial complexation has also been demonstrated to assemble strong interfacial interaction between charged molecules. High charge densities of negatively charged CNF and positively charged chitosan benefit interaction between them. Filaments exhibited tensile strength as high as 1290 MPa. (Cai et al. 2020)

2.3 Parameters for nanocellulose based filament fabrication

Both properties of nanocellulose and spinning parameters affect the filament properties. Especially, charge density, solid content and structure of nanocellulose influence the mechanical properties of the nanocellulose based filaments. (Lundahl et al. 2016; Zhang and Liimatainen 2018) Generally, alignment of the nanofibers inmprove mechanical properties of filaments. To align nanofibers, magnetic field (Pullawan et al. 2012) and electric field (Bordel et al. 2006) can be used. However, controlling spinning speed is the easiest way to create shear forces, thus align nanofibers. Filament properties can also be

controlled via adjusting the other spinning conditions such as stretching, coagulation and drying. Depending on the filament application, the priorities regarding the CNF and spinning process might change and be adjusted. (Lundahl et al 2017)

2.3.1 Properties of nanocellulose

Lundahl et al. (2016) investigated the influence of the CNF solid content (which affect directly to viscosity) and surface charge on filament wet spinning. They compared unmodified CNF and TO-CNF. Spinnability of CNF depends on solids content of hydrogel. On a scale of 1% - 10% solid fraction of 2% produced filaments with the highest degree of orientation, thus highest tensile strength and Young's modulus. Also, difficulties in spinning were observed when solid content was too low or too high, such as 1% or 10%, respectively.

Increased CNF surface charge can improve the mechanical properties of filament. During wet spinning TO-CNF filament represent higher orientation than unmodified CNF. This is because of higher CNF surface charge and aspect ratio, which cause attachment and osmotic pressure between nanofibers. Additionally, increased degree of polymerization promotes spinnability, thus filament fabrication using a high DP CNFs is easier and filaments are stronger and stiffer (Lundahl et al. 2016; Michud et al. 2015).

2.3.2 Spinning rate

To improve mechanical properties of filaments, it is advantageous to apply shear force on wet spinning while the CNF flowing through the spinning needle. Spinning speed and inner diameter of needle are the main details that control shear stress inside the needle. The shear stress is corresponding to the spinning speed and is inversely proportional to inner diameter of needle. (Kim et al. 2019) The increasing shear rate aligns the fibers into filament axis and higher degree of surface contacts between CNFs are occurred, which supply a better opportunity to make hydrogen bond interactions. This makes the structure of filaments more oriented, thus increasing the stiffness and tensile strength. (Iwamoto et al. 2011; Kafy et al. 2017) According to Kim et al. 2019, optimal conditions were found to be 1700 cm/min of spinning speed and 380 μm of inner diameter of needle.

Kafy et al. (2017) investigated the correlation between spinning speed and nanofiber orientation. Spinning speed increase from 2.0 ml/min to 10.0 ml/min resulted orientation index increase from 0.64 to 0.66, respectively. Similarly, Young´s modulus and tensile strength increased from 13 GPa and 224 MPa to 17 GPa and 250 MPa, respectively. However, as tensile strength and Young´s modulus increased, strain at break decreased from 13% to 9.2%.

On the contrary, while using interfacial complexation the mechanical properties of TO-CNF/chitin nanocrystal decreased as drawing speed increased. In order to offer enough time for complexation of oppositely charged particles, slow speed is necessary. With a speed of 40 mm/min, tensile strength of 184 MPa and Young's modulus of 8.3 GPa were obtained for filament from TO-CNF/chitin nanocrystals. (Zhang et al. 2020b)

In case of wet spinning by flow focusing, an extensional flow in the core is created as the sheath/shell flow have higher velocities than the core flow. The sheath flow promotes gelatinization of CNF, thus enable the locking of the aligned nanofiber structure before coagulation. This improves filament orientation, following increased tensile strength and stiffness. (Lundahl et al. 2017)

2.3.3 Coagulation

Coagulation refers to a counter-diffusion of solvents occurring between CNF and coagulant as the cellulose solution contacts the coagulation bath. Solvent removal from CNF and penetration of coagulant into the CNF solution causes the CNF losing its solubility and results in semisolid CNF filaments. (Zhang et al. 2005) It has been demonstrated that there is a clear effect between coagulation type and structural and mechanical properties of the spun filaments. Previously two types of coagulants have been employed in wet spinning of CNF: organic solvents such as ethanol, acetone, dioxane, tetrahydrofuran and isopropyl alcohol; and aqueous electrolyte solution such as $CaCl_2$, NaCl and HCl. (Lundahl et al. 2017; Wang et al. 2019)

Wang et al. (2019) compared different coagulants for TO-CNF coagulation during wet spinning. A correlation between the coagulation type, filament morphology, CNF orientation and physical properties was found. Also, coagulation and drying times, washing and continuous spinnability depends on coagulant. It was observed that to obtain

filaments from TO-CNF, nanofiber aggregation in the coagulation bath is required either by physical aggregation i.e. by hydrogen bonding using organic solvent or by chemical complexation. Filament coagulated in aqueous electrolyte solution ($CaCl_2$ or HCl) indicated better tensile strength, thermal stability, water resistance property and more circular cross-section compared to filament produced in organic non-solvent (acetone and ethanol). Presence of calcium cations enhance the coagulation by complexation and cross-linking and thus greatly enabled cellulose filament formation. Furthermore, continuous spinning of filaments formed in $CaCl_2$ and HCl coagulation baths was successfully achieved with a winder while filaments coagulated in ethanol and acetone had not continuous spinnability. This was explained by weaker gel that does not support filament weight while it is taken up from bath. (Wang et al. 2019)

$CaCl_2$ as a coagulant for TO-CNF causes interfibrillar interactions by counterion condensation. Presence of functional groups, such as COO^-Na^+, on the surface of the CNF facilitates metal interaction. In this so-called ion mediated wet spinning, filament formation is occurring by crosslinking with calcium cations (Ca^{2+}). Ca^{2+} diffuse in the TO-CNF dispersion and replace Na^+ in the surface. This creates ionic bonds between carboxylic groups with negative charge and Ca+. When coagulant diffuse in CNF, in the meanwhile water in CNF diffuse in coagulant. Diffusion rates of coagulant and water effect the morphology of filament surface. (Wang et al. 2019, Kafy et al. 2017)

In addition to coagulation type, also coagulation rate determines CNF orientation (Lundahl et al. 2018). Coagulation time has been reported to be from 5 min to 12 h. It is considered that at least several minutes may be necessary for coagulation of CNF dispersion and it has been stated that coagulation is rate-limiting in wet-spinning. (Lundahl et al. 2017) However, Wang et al. (2019) reported that TO-CNF filaments can immediately be collected from aqueous electrolyte solution such as $CaCl_2$, due coagulation phenomenon occurring upon contact with the coagulant. Coagulation time was estimated to be 5 s for acetone and 30 s for ethanol.

2.3.4 Stretching

Mechanical stretching of CNF filaments axially aligns nanofibers and cellulose polymer chains along the filaments and increase hydrogen bonds between CNFs, which results more oriented structure. Generally, as fiber alignment is improving tensile strength and

stiffness while decreasing breaking elongation. (Lundahl et al. 2017; Kim et al. 2019) Previously filament stretching has implemented using computer controlled wet-stretching (Torres-Rendon et al. 2014), physical stretching using shifting device (Kafy et al. 2017) or winding the filament faster than extrusion speed (Lundahl et al. 2018). Drawing during spinning is defined by the drawing ratio (DR), that is ratio between filament winding velocity and spinning velocity determined by equation 1. Drawing ratios over 1 result in stretching. (Lundahl et al. 2017)

$$DR = \frac{v_{winder}}{v_{needle}}, \quad (1)$$

where v_{winder} corresponds to the winding speed (i.e. drawing speed) [m/min] and v_{needle} corresponds to the extrusion speed of the dope in the needle [m/min] (Lundahl et al. 2018).

Figure 8 assembles various studies related to the stretching effects. In all of studies TO-CNF from wood was wet spun into filaments and stretched using stretching device. Although the processes were not identical, thus not completely comparable with each other, in general stretching can be seen to increase tensile strength and Young's modulus. 20% stretching have produced strongest filaments with Young's modulus of 37.5 MPa, and tensile strength of 543.1 MPa. Without stretching filaments only had Young's modulus of 24.3 MPa, and tensile strength of 492.6 MPa. (Kim et al. 2019) Furthermore, stretching ratios higher than 30% are unreliable and lead to fracture of filament (Torres-Rendon et al. 2014).

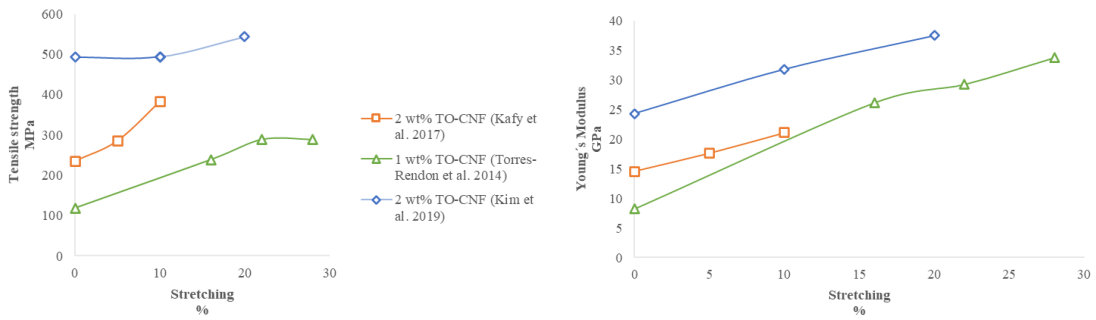

Figure 8. Tensile strength and Young's modulus as a function of stretching.

Earlier filament stretching have mainly been performed separately from spinning, which is not possible in case of continuous process. To achieve maximum performance of

stretching, it needs to be integrated into real up-scale spinning process (Torres-Rendon et al. 2014). Inferior wet strength of hemisolid CNF filaments in the coagulation bath is challenging for keeping the filaments under tension i.e. stretched throughout the filament fabrication process. (Lundahl et al. 2017, Lundahl et al. 2018). According to Vuoriluoto et al. (2017) wet-spun TO-CNF had strain at break of 0.07% and tensile strength of 0.44 MPa in wet state, while in the dry state 2.8% and 237 MPa, respectively.

Drawability has been confirmed to correlate with the DP of cellulose. High DP improve spinnability thus lead higher drawing ratios. (Michud et al. 2015) Drawing ratios of 1-3 for CNF filaments are close to the values generally applied in the viscose process (DR of 1-2.5) with a DP of 300 for viscose. They are still much lower than drawing ratio for lyocell (DR of 8.4), which DP is 550. To increase drawing that high, CNF aspect ratio extension would be required by modifying or blending CNF with a high- DP polymer or using hybrid systems. (Lundahl et al. 2017)

2.3.5 Washing

To remove non-reacted coagulant from the filament surface, washing step is needed. Washing with DI water has shown effectively remove absorbed $CaCl_2$ coagulant from the TO-CNF filament. (Kafy et al. 2017) Reyes et al. (2020) stated that washed core-shell filaments (TO-CNF/PIL) have higher tensile strength, toughness and elastic modulus both in wet and dry state compared to unwashed filaments.

Washing of TO-CNF filaments has been performed by dipping them in fresh water using 4 cycles and immersed in water for 10 min and 2 h respectively, which was necessary to remove the excess salts (Wang et al. 2019). Also longer, such as 1 day, immersion into water has been reported (Kim et al. 2020).

2.3.6 Drying

Fibers tend to flatten upon drying in contact with a surface of winder, thus fiber drying before uptake on a winder is necessary (Nechyporchuk et al 2019). Also drying temperature is important parameter since it promotes hydrogen bonds with CNFs after wet spinning. Formation of microbubbles is occurring rapidly as drying temperature is increasing, which can negatively affect the formed filaments. Therefore, the optimal

drying temperature, which facilitates hydrogen bond formation and ion linkage among CNF for wet spinning was found to be 30 °C (compared to 60 °C and 90 °C), as it exposes the greatest mechanical properties for filaments. (Kim et al. 2019)

Drying has also been performed at 105 °C for 1 h (Iwamoto et al. 2011). Increase in drying temperature caused only a little effect on the mechanical properties of the filaments. Thus, high temperature could be used to decrease drying time without negatively affecting the filaments. (Ludahl et al. 2017) Similar results were obtained in the dry spinning process. The effect of heating of filaments was investigated at 210 °C, 320 °C and 430 °C. Drying was executed using a heat gun at 10 cm distance from the winder. Drying temperature negligible influenced the structure and tensile properties of dry-spun CNF filaments. Thus, the drying unit of CNF filament spinning can be implemented at high temperatures to save time and increase production rate. (Ghasemi et al. 2017)

2.4 Continuous processes for production of nanocellulose based filaments

In the wet state CNF filaments frequently break, preventing continuous spinnability (Lundahl et al. 2018b). Only in a few studies filaments have been produced continuously (i.e. collected on a winder). Lundahl et al. (2018) continuously produced filaments using wet spinning with drawing. CNF filaments were spun into coagulation bath and collected on a winder (diameter of 6 cm) under heating with hot air. Core-shell structure was essential for the filament, as the filament broke in the absence of a shell. Cellulose acetate and guar gum were effective supporting polymer as a shell material and made possible the continuous filament formation. Core-shell structure formed from cellulose nanofiber (1 wt%) and cellulose acetate (15%) (CNF/CA) could continuously wet spun into acetone at a maximum rate of 33 m/min, in which case drawing ratio (DR) was 3 (CNF extrusion speed was 11 m/min). Thus, the drawing was created by winding the filaments faster than extrusion speed. It was noticed, that fast, even immediately, coagulation is required to produce strong filament, which can resist stretching.

Core-shell filaments have also been produced using TO-CNF as a core and protic ionic liquid (PIL) as a shell, as mentioned earlier in the section 2.2.3. Steady flow of 0.6 and 2 mL/min for core and shell syringes, respectively, and the filament take-up speed on the 6

cm winder was 68 cm/min causing DR of 1.15, were employed. 2 cm air gap between needle and coagulation bath was assumed to allow cellulose orientation and drawing. (Reyes et al. 2020)

Nechyporchuk et al. (2019) developed a continuous wet spinning process based on microfluidic flow focusing from sulphated CNCs and non-purified grades of carboxymethylated CNFs. Process involved microfluidic device, coagulation bath and winder. Aqueous suspension of ionized nanocellulose were aligned with first sheath flow (H_2O) following alignment and coagulation with second sheath flow (HCl). This spinning resulted in the formation of thin and continuous suspension. Suspension was extruded into the coagulation bath for the additional coagulation. Filaments were successfully produced and collected from the bath on a winder. Filaments possessed a tensile strength of 330 MPa, Young's modulus of 18 GPa, and strain at break of 5.4 %.

3 EXPERIMENTAL PART

The intention of the experimental part of this work was to investigate if it is possible to produce continuously core-shell filaments from nanocellulose. The idea for this work is based on previous study, in which nanocellulose based filaments were produced using oppositely charged cellulose materials by interfacial complexation (Zhang and Liimatainen 2018). In this study, wet spinning and interfacial complexation was combined with a view to produce filament purely from CNF with a continuous laboratory scale process.

The experimental part composes of two main sections: development of the process by integrating the required process steps and optimization of the manufacturing process. First, different types of CNFs for filament fabrication were prepared. Then, continuous process, i.e. process containing core-shell wet spinning, winding and drying steps, for filament fabrication was developed. Furthermore, process was optimized by modifying following process parameters: spinning speed, drying temperature and needle size. Additionally, the effect of washing and stretching of filaments were investigated. Fabricated filaments were characterized by optical and electron microscopy, and tensile tests were performed in order to compare the mechanical properties of filaments.

3.1 Materials

In this study, birch pulp sheet from UPM was used as a cellulose raw material for nanocellulose production. Sodium periodate (purity ≥99%), glycerol (≥99.5%), sodium bromide (>99%), sodium hypochlorite (14%), ethanol (≥96%) and calcium chloride (≥96%) were obtained from VWR. Sulfamic acid (≥99.5%), urea, lithium chloride (≥99%) were purchased from Sigma Aldrich. Aminoguanidine hydrochloride (≥98%), TEMPO (≥98%) and succinic anhydride (≥95%) were obtained from TCI. Deionized water was used throughout the study.

3.2 Preparation of nanofibers

3.2.1 Modification of cellulose

Deep eutectic solvents were used to produce functionalized cationic and anionic cellulose nanofibers. Additionally, anionic TEMPO-oxidized CNFs were produced as references. For the synthesis of cationic nanocellulose, 30 g (abs.) of pulp was soaked with 1000 g of water for overnight. Pulp was disintegrated according to ISO 5263-1:2004. Water was added until the total mass was 2000 g, the pulp was disintegrated at 30 000 rpm and filtrated. First, dialdehyde cellulose (DAC) was obtained by sodium periodate ($NaIO_4$) oxidation. 20 g (abs.) of pretreated pulp was diluted with 2000 g of water. Suspension was heated to 55 °C in the water bath and covered thoroughly with aluminium foil. 16.4 g of sodium periodate was added and left to react with cellulose while continuously stirring for 3 h. The product was filtered and washed with 2 000 ml of water. The DAC was further cationized with aminoguanidine hydrochloride in DES. DES was first prepared by mixing 105 g aminoguanidine hydrochloride and 175 g glycerol in a molar ratio of 1:2 at 90 °C until a clear liquid was formed. The temperature was adjusted to 80 °C and 14 g DAC (abs.) was added. The DES-DAC mixture was mixed for 10 min, subsequently 250 ml ethanol was added. Suspension was filtered and washed twice with 500 ml of ethanol.

Anionic celluloses were produced using sulfonation and succinylation. Sulfonation was performed by mixing the components of DES, 21.56 g of sulfamic acid and 26.6 g of urea, in an oil bath at 80 °C at a molar ratio of 1:2. After clear solution was obtained, 12 g of cellulose (abs.) was added (3 times molar excess of sulfamic acid compared with the AGU of cellulose) and immersed in DES. Temperature was increased to 150 °C, and the reaction was allowed to proceed for 30 min. Following that, mixture was cooled for 5 min and reaction was ended by the addition of excess of water. Mixture was filtrated and washed with water until the filtrate was neutral.

Succinylation was performed by mixing the components of DES, 438.15 g of urea and 61.85 g of lithium chloride, at a molar ratio of 5:1 in an oil bath at 90 °C. After the clear solution was obtained, temperature was decreased to 70 °C and 10 g (abs.) of pulp and 37.03 g of succinic anhydride at molar ratio of 1:10 were added into solution and continuously stirred for 6 h. Subsequently the mixture was removed from the oil bath and

500 mL ethanol was added. Mixture was filtered and washed with 500 mL of ethanol and 2000 mL of water.

For TEMPO-mediated oxidation 10 g (abs.) of pulp was dispersed into 1000 mL water using Ultra-Turrax mixer with speed of 10 000 rpm for 2 min. 0.16 g of TEMPO and 1 g of sodium bromide were added and dissolved to pulp dispersion. After dissolution, 66.6 mL of 15% NaClO solution was slowly added within 4 h using a dropper. Simultaneously pH was controlled at a value of 10 using dilute NaOH. After 4 h, solution was reacted for 1 h. Following that 10 mL of ethanol was added to terminate the reaction and suspension was filtered and washed with water until the filtrate was neutral.

3.2.2 Nanofibrillation of cellulose

Pretreated celluloses were diluted to a consistency of 2 wt% in water and pH was adjusted to 7. Celluloses were disintegrated by passing once at a pressure of 1500 bar through the 400 and 100 µm chambers of a microfluidizer (M-110EH-30, Microfluidics, USA). After nanofibrillation, samples were taken from the suspensions and dried at 105 °C overnight to determine the dry matter content.

3.3 Development of filament fabrication process

The main intention of this study was to investigate if filaments could be produced continuously using oppositely charged nanofibers using interfacial complexation and wet spinning. Initially system comprised of syringe pump (Syringe two, NE-4000, New Era), coaxial needle, coagulation bath and winder, shown in Figure 9. For a steady flow, there was a flow barrier at the front of the coagulation bath, and the flow of the coagulant was controlled using hose pump with constant rotation speed of 85 rpm.

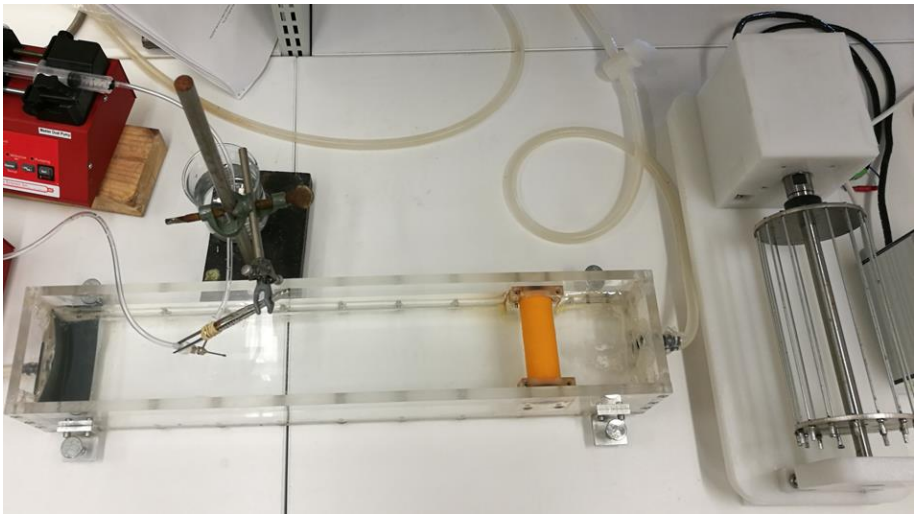

Figure 9. Initial system before process development.

The most important task was to connect a winder to the system in order to create continuous process, in which long and unbroken filaments could be fabricated. Furthermore, drying stage was introduced to the process. Process was self-made and -developed by experimental research. The updated system comprised of two syringe pumps, coaxial needle, coagulation sink, roller, dryer and winder, as shown in Figure 10a. This layout ensured continuous filament fabrication without filament rupture during process. Flowchart of the process is shown in Figure 10b. Next, the final process and working principles are described thoroughly.

Figure 10. a) Image of the final core-shell spinning system after process development comprising of two syringe pumps, coaxial needle, coagulation sink, Teflon roller, hot air gun and winder, and b) flowchart of the process.

To fabricate core-shell filaments, oppositely charged cellulose nanofibers were used. Originally, four different CNFs, i.e. cationized dialdehyde cellulose nanofibers (abbreviated hereafter as CDAC-CNF), and anionic sulfonated nanofibers (S-CNF), succinylated nanofibers (SC-CNF) and TEMPO-oxidized nanofibers (TO-CNF) were synthesized. However, only TO-CNF, S-CNF and CDAC-CNF were used for filament fabrication since SC-CNF showed to be unsuitable because water separated from SC-CNF during extrusion. TO-CNF and S-CNF were centrifuged at 5 000 rpm for 10 min to remove excess air from the aqueous suspensions. The bubbles caused by dissolved air were assumed to negatively affect the structure of filament. Figure 11 displays appearance of TO-CNF before and after centrifugation.

Figure 11. 1.5 wt% TO-CNF a) before, and b) after centrifugation.

After centrifugation, CNFs were poured into 50 mL syringes, in which possibly re-formed air was removed, before injecting to two 10 mL syringes. Core-shell filaments were attempted to be fabricated so that cationic CDAC-CNF was as a core and anionic CNFs as a shell, and vice versa. It was noticed that filament with cationic core and anionic shell broke easily and were nearly impossible to lift to the winder. When the core-shell structure was reversed, so that TO-CNF and S-CNF were on the core and CDAC-CNF in the shell, filaments did not break that easily and were able to be lifted on the winder immediately. Thus, 10 mL syringe with anionic CNF was connected to core and cationic CDAC-CNF to shell section of the coaxial needle. Syringes extruded CNF using two syringe pumps at controlled speed into $CaCl_2$ coagulation bath. Initial syringe pump was not able to pump CNF with high consistency (i.e. over 1.5 wt%), thus, pump was replaced with two parallel more powerful syringe pumps (Syringe one, NE-1010X, New Era).

There was around 2 cm air gab between the needle tip and surface of coagulant bath (Figure 12b) to ensure possible CNF alignment and complexation. Filament moved approximately 30 cm in coagulation bath (Figure 12a) before they were grabbed from bath by hand and lifted through a roller to directional hot drying air and further to the rotating winder. Coagulation time was set between 15 s – 1 min depending on the spinning speed. Filaments were collected immediately from the coagulant bath when they were long enough to be drawn to a winder.

Drying before winding reduced filament flattening on a winder, and was merged into process. Hot air gun was used and different positions for the gun was tested. Drying was the most effective as hot air gun was around 2 cm above filaments and air was directed slightly downward (Figure 12c). This also prevented filaments from burning because hot air did not point directly on winder. It was observed that very high temperature (>500 °C) was essential to dry the skin of the filaments before winding. However, the filaments sticked to the winder and thus were flattened and broke when they were removed from the winder. To avoid this, rapeseed oil and Teflon spray (WD-40 PTFE-dry lubrication spray) were effective to prevent filament sticking on winder and enabled to keep their circular structure.

Winder with diameter of 100 mm and different drawing speeds were tested in different heights and positions to investigate proper positioning of winder. The winder was placed on a podium and set slightly above the coagulation bath. It was also flipped sideways. This position and height were essential since they allowed filament to be lifted from the coagulation bath before the roll (orange roll in figure 12a) in the coagulation bath. Uptake before the roll was essential since filaments tended to adhere on the lower surface of it. Winder flipped sideways prevented filaments adhered on the plate under winder as filaments were lifted to winder. It was also observed that the roller between the coagulation bath and winder was essential to support weak wet filaments and prevent them from breaking when they were lifted on a winder. Additionally, support was needed because drying air pushed filaments away without roller. Too high friction between filament and roller tend to break the filament, which had a low wet strength. Small diameter of the roller provided small contact area and low friction between filament and roller. Teflon tube with diameter of ca 1 cm was chosen as it was small and had a high heat resistance. Additionally, tube was covered with Teflon spray for filaments fabricated using only TO-CNF as they started to get stuck in it.

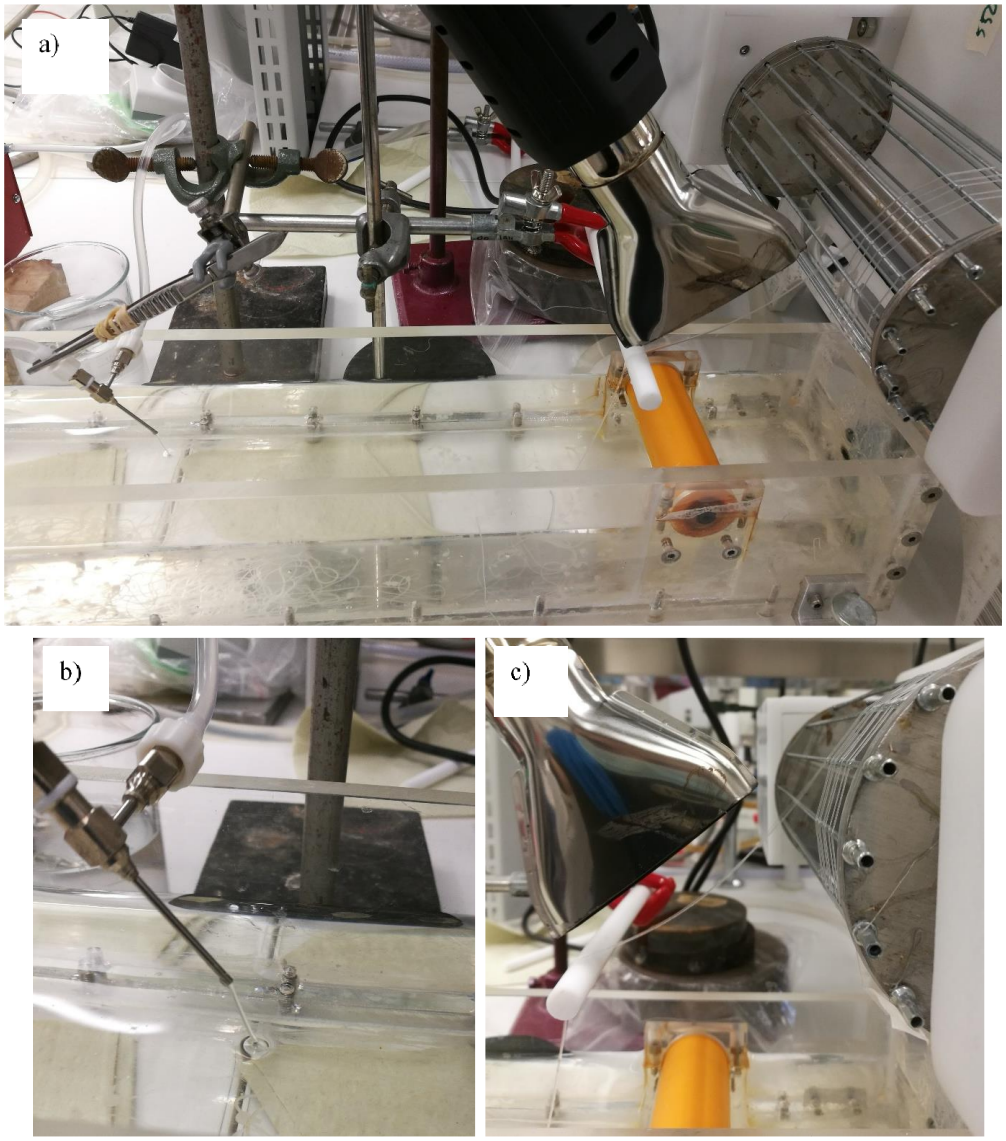

Figure 12. The process layout for a) coagulation, drying and winding, and a closer look for a b) needle and c) dryer positions.

Drawing speed was adjusted so that the filament was tight from the tip of needle to the winder, and filaments got visibly thinner, which indicated filament stretching. This can be seen in Figure 12b, in which filament is slightly diagonal due to drawing. The winder was occasionally covered with Teflon spray to avoid filaments get stuck on it. It was also manually moved so that filaments were placed beside to each other. At last, filaments were collected from the winder on a roller for a storage. (Figure 13)

TO-CNF and S-CNF were successfully used to fabricate filaments with cationic CDAC-CNF using developed process based on interfacial complexation with core-shell wet spinning. Fabricated filaments are referred to their names containing first the core,

following the shell, such as TO-CNF/CDAC-CNF, which refers to filament with TO-CNF as a core and CDAC-CNF as a shell. Thus, fabricated core-shell filaments were TO-CNF/CDAC-CNF and S-CNF/CDAC-CNF. Furthermore, filaments purely based on TO-CNF (TO-CNF/TO-CNF) were produced as a reference for the other two DES based filaments. Figure 13 shows the fabricated filaments. For TO-CNF/CDAC-CNF consistencies of TO-CNF and CDAC-CNF were 1.8 and 1.9 wt%, respectively, for S-CNF/CDAC-CNF consistency of both CNFs were 1.6 wt%, and for TO-CNF/TO-CNF 1.8 wt%.

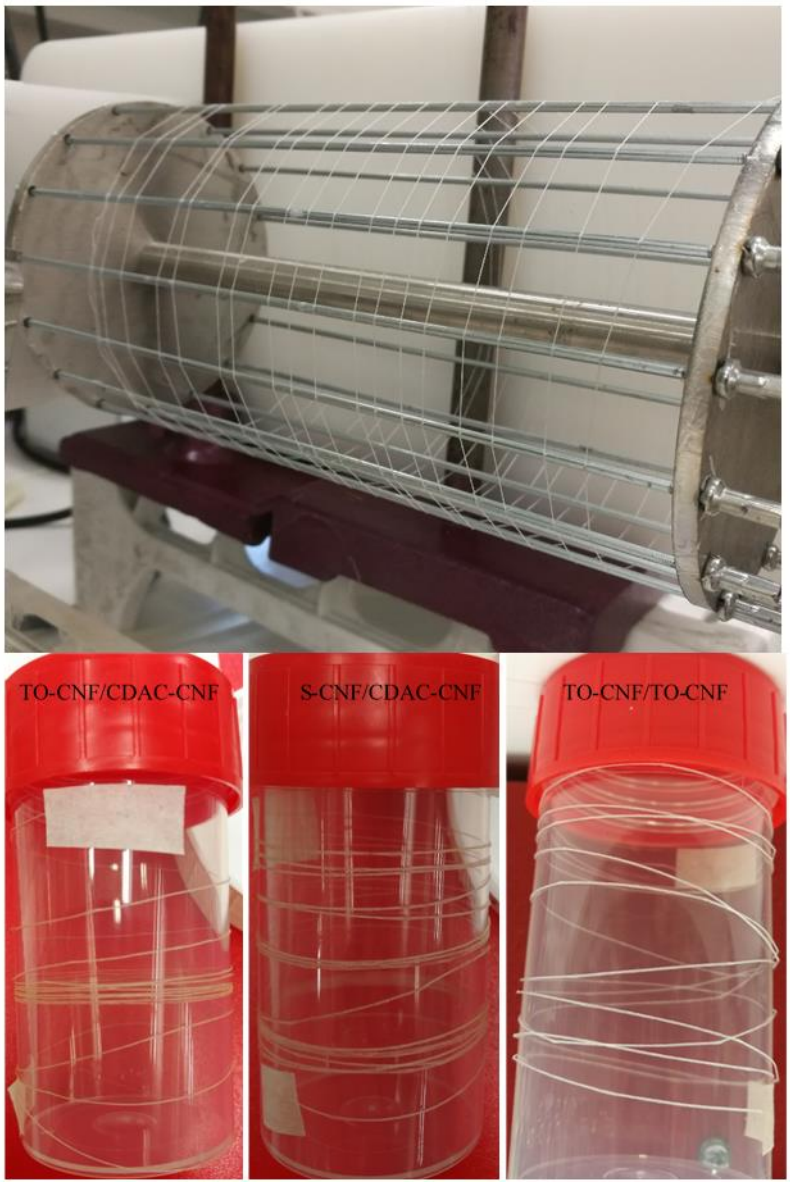

Figure 13. Filament collected on a winder (above), and three different filaments collected on storage roller (below).

3.4 Optimization of filament production process

To optimize the process, different drying temperatures (450 – 650 °C), spinning speeds (0.250 – 0.750 mL/min), washing and different size of needle (20/16G and 22/18G) were applied to discover the most suitable process conditions for filament fabrication. In situ stretching was also utilized at the process. Filaments were stretched by winding the filament as fast as filament was tight between needle and winder. To compare the effect of the stretching, also reference filament without stretching was fabricated.

3.4.1 Drying temperature

Filaments were dried under different drying temperatures, 450, 500, 550, 600 and 650 °C, to investigate the effect of drying temperature on mechanical properties. Drying was done using a hot air gun mounted at around 2 cm distance from the moving filaments. Temperatures are ones set at the heat gun, while the accurate temperature on filaments are likely lower. Accurate temperatures were not investigated. Constant spinning speed of 0.350 mL/min was used.

3.4.2 Spinning speed

The effect of spinning speed was studied by changing the feeding speed of core and shell syringes. Spinning speeds of 0.250, 0.350, 0.450 and 0.550 mL/min were used when speed of core and shell were equivalent, i.e. spinning speeds of core and shell were equal. Additionally, spinning speed of shell was increased while speed of core was constant. For TO-CNF/CDAC-CNF and TO-CNF/TO-CNF spinning speeds 0.350/0.450, 0.350/0.550 and 0.350/0.650 mL/min were used. First number express the spinning speed of core and latter the speed of shell. For example, 0.350/0.450 mL/min refers to that feeding speed of core was 0.350 mL/min and speed of shell was 0.450 mL/min. For S-CNF/CDAC-CNF, spinning speeds of 0.450/0.550, 0.450/0.650 and 0.450/0.750 mL/min were used.

Difference between the speed of core and shell is expressed as a ratio between them. 0.350/0.450 and 0.450/0.550 mL/min are connected to a ratio of 1/1.2, in which spinning speed of shell is around 20% higher than spinning speed of core. Similarly, spinning speeds of 0.350/0.550 and 0.450/0.650 mL/min; and 0.350/0.650 and 0.450/0.750

mL/min are expressed as ratios of 1/1.5 and 1/1.7, respectively. Constant drying temperature of 650 °C was used in the experiments.

3.4.3 Washing

Effect of washing on filament properties was also studied. After filament fabrication, three different pieces of filaments, TO/CDAC, S/CDAC and TO/TO fabricated with spinning speed ratio of 1/1.2, were immersed in water for 24 h, dried at 650 °C and collected on a winder. Drying was performed at the same time as filaments were taken up from water on a winder, similarly to drying in continuous process.

3.4.4 Needle size

For most of the filaments, the needle type was 20/16G, which refers to a needle made of an internal needle (inner diameter of 0.584 mm and outer diameter of 0.889 mm) and an external needle (inner diameter of 1.19 mm and outer diameter of 1.65 mm). To compare the influence of needle size, smaller needle was also used. The smaller needle, 22/18G, had an internal needle with inner diameter of 0.406 mm and outer diameter of 0.711 mm and an external needle with inner diameter of 0.84 mm and outer diameter of 1.24 mm. TO-CNF/CDAC-CNF and S-CNF/CDAC-CNF were fabricated using 22/18G needle, core-shell spinning speed ratios of 1/1, 1/1.2, 1/1.5, and 1/1.7 and a constant drying temperature of 500 °C.

3.4.5 Stretching

Filaments were stretched so that filaments were tight from the tip of a needle to the winder. The effect of stretching was investigated by means of drawing ratio between drawing speed and spinning speed. Drawing ratios of the filaments were calculated using equation 1.

3.5 Fabricated filaments

Table 2, in the Appendix 1, summaries the prepared filaments. It presents filament composition and consistencies of CNF suspensions. Spinning speeds are expressed for both core and shell in terms of mL/min. Drawing speed is expressed for both winder level (e.g. W4, which refers to winder level 4) and corresponding drawing speed in cm/min.

UST refers to unstretched filament. Additionally, drying temperatures and if post-washing was implemented, are expressed in Table 2.

3.6 Characterization of cellulose nanofibers

3.6.1 Polyelectrolyte titration

The surface charge density of CNFs was determined using the polyelectrolyte titration method with a particle charge detector (Mütek PCD 03). The CNF suspensions were diluted with water into 0.01% solution. 10 ml of suspension was titrated with the sodium polyethylene sulfonate (PES-Na) or polydiallyldimethylammonium chloride (Poly-DADMAC) depending on the charge of the sample. The charge density was calculated based on the consumption of titrant using equation 2.

$$q = \frac{Vc}{w_t}, \tag{2}$$

where q corresponds to the charge [eq/g or meq/g], V is the consumption of the titrant [L], c is the concentration of the titrant [eq/L] and w_t is the solid content of the sample [g].

3.6.2 Transmission electron microscopy

The morphological features of TO-CNF, S-CNF and CDAC-CNF were analyzed using a transmission electron microscope (TEM, JEOL JEM-2200FS, Japan) at an acceleration voltage of 200 kV. TEM samples were prepared on top of carbon coated copper grid. Anionic CNF samples were prepared by dropping 7 µL of 0.1% poly-L-lysine, then 7 µL of 0.01% CNF, and finally 7 µL of 2% uranyl acetate to the grid. Each solution was allowed to react 1 minute on a grid before excess of poly-L-lysine and CNF was dried with filter paper. Finally, grid was sinked under water to remove excess of uranyl acetate. Cationic CNF sample was prepared similarly, however without poly-L-lysine. The width distribution of the CNF samples were measured using ImageJ analysis software.

3.7 Characterization of filaments

3.7.1 Optical microscopy

The morphological features of filaments were analyzed using optical microscope (Leica MZ6 equipped with a Leica DFC420 camera, Germany).

3.7.2 Field emission scanning electron microscopy

Cross-sectional structure of filaments was observed using a field emission scanning electron microscope (FESEM) (Zeiss Sigma, Germany) at an acceleration voltage of 5.0 kV. The samples were sputtered with platinum before observation.

3.7.3 Mechanical tests

The mechanical properties of the filaments were measured by a universal testing machine (Inston 5544, USA) equipped with a 200 N load cell. Before the sample preparation, the average of the filament diameter was measured by optical microscope (Leica MZ6 equipped with a Leica DFC420 camera, Germany). For each filament, average values of 20-30 measurement were calculated. Filaments were preconditioned in a relative humidity of 50% at room temperature for at least 24 h prior to the testing and measured at the same conditions. The samples were prepared by cutting 4-6 pieces from the filament with the length of 35 mm. Pieces were clamped between tape to prevent filament slippage. Additionally, flat parts of the filaments were placed under the tape to prevent flat parts, assumed to be weaker, from being tested. For the testing, the gauge length was set to 15 mm and the samples were measured at a strain rate of 5 mm/min with a pre-load of 0.01 N. The mechanical properties in terms of tensile strength, Young's modulus and strain at tensile strength were obtained directly from the test results. Instead of strain at break, strain at tensile strength (i.e. strain attained at the highest point of the stress-strain curve before fracture) was chosen since test did not present strain at break for every specimen. For each sample, average values and standard deviations of 4-6 measurements were presented.

4 RESULTS AND DISCUSSION

The experimental part is divided into filament spinning process development and process optimization sections. First, it was investigated how the core-shell filaments can be produced in a continuous process utilizing interfacial nanoparticle complexation and wet spinning. This part focused on integrating different unit operations in the spinning process. Next, the influence of process parameters, drying temperature, spinning speed, needle size and washing on the spinning process was investigated to optimize the process. Microscopy and tensile strength tests were used to analyse the structure and mechanical properties of filaments. All fabricated filaments and their corresponding process parameters and properties are listed in Table 2 in Appendix 1 and Table 3 in Appendix 2.

4.1 Characterization of nanofibers

In this thesis, four different types of charged nanofibers, CDAC-CNF, S-CNF, SC-CNF and TO-CNF, were prepared for filament production. CDAC-CNF, S-CNF and SC-CND were based on DESs chemistry. The characteristics of the nanofibers are shown in Figure 14 and Table 1. All CNFs exhibited elongated nanofibrillar morphology. CDAC-CNFs showed existence of some larger fiber aggregates, which can be seen in bottom left in Figure 14a, whereas S-CNF and TO-CNF consisted mainly of individual nanofibers. CDAC-CNF had an average width of 4.7 ± 1.6 nm, S-CNF width of 4.5 ± 1.8 nm, and TO-CNF width of 3.0 ± 1 nm. The charge density was 0.97 meq/g for cationic CDAC-CNF, and -0.73 meq/g for anionic TO-CNF, -1.38 meq/g for S-CNF and -0.27 meq/g for SC-CNF. Width of SC-CNF was not measured because it was unsuitable for filament fabrication.

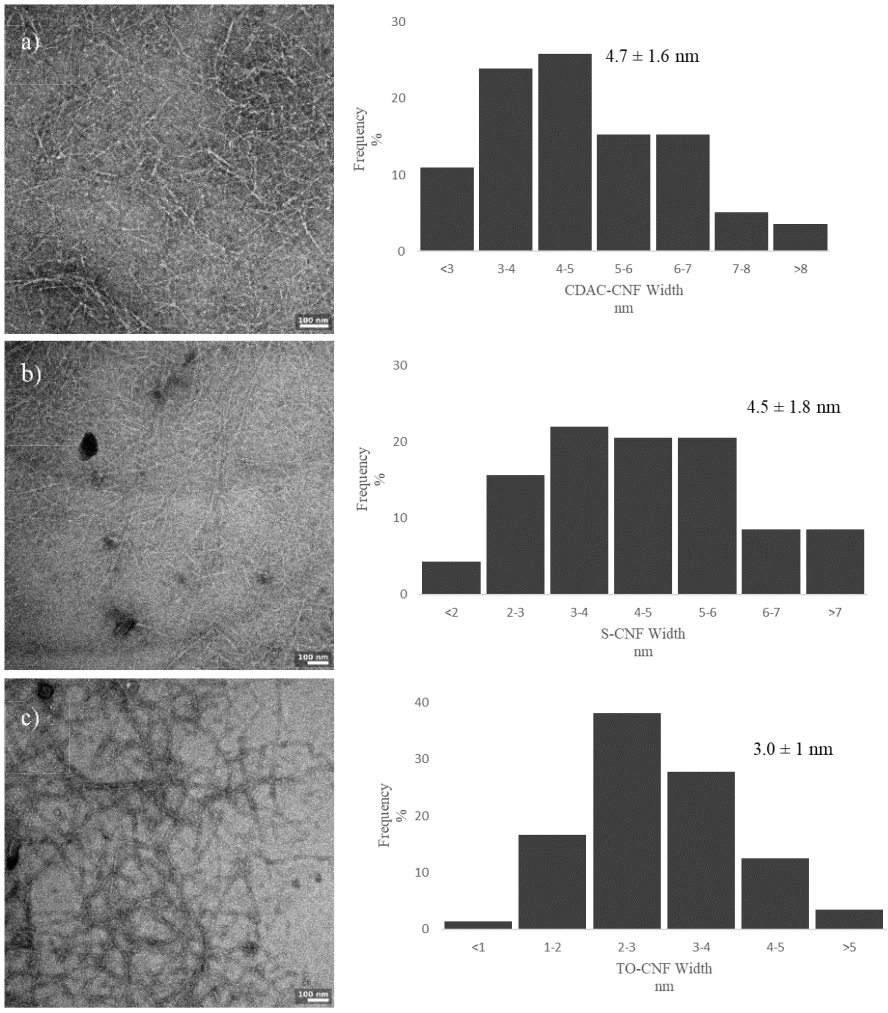

Figure 14. TEM images of a) CDAC-CNF b) TO-CNF and c) S-CNF and their corresponding width distribution graphs. For each sample, 150 measurements were conducted for width distribution.

Table 1. Characteristics of nanofibers.

CNF	Charge	Charge density (meq/g)	Width (nm)
CDAC-CNF	Positive	0.97	4.8±1.6
TO-CNF	Negative	0.73	3.0±1.1
S-CNF	Negative	1.38	4.5±1.8
SC-CNF	Negative	0.27	-

4.2 Fabrication process for filaments

The main purpose of this thesis was to develop continuous fabrication process for core-shell filaments based on solely on cellulose nanofibers. Process was self-made by experimental research, being the most challenging part of the thesis. Air removal from CNFs, suitable combinations of CNF, filament supportive roller before winding,

minimization of friction, and Teflon surface on the winder were the key elements that enabled continuous filament fabrication.

The developed fabrication process is described in detail in section 3.3. Briefly, oppositely charged CNF suspensions were loaded in two syringes, that were connected to the core and shell sections of a coaxial needle, and were further extruded through a needle at a controlled speed into the $CaCl_2$ coagulation bath. After, approximately 30 cm travel in the bath, filaments were collected through drying section on a winder, which was moved manually so that filaments were placed next to each other. A roller between coagulation bath and winder was necessary since it supported filaments for breaking during lifting to the winder and enabled proper drying. Filaments were collected around the roll for storage. Flattening of the filaments in the winder was reduced using Teflon surface on the winder.

Air removal by centrifugation of TO-CNF and S-CNF suspensions was mandatory because air caused filament breaking already at the end of a needle. CDAC-CNF was less viscous, thus air removal was not required. Different core-shell filaments were attempted to be fabricated so that cationic CDAC-CNF was as a core and anionic CNFs as a shell, and vice versa. First, a structure consisting of CDAC-CNF as a core and anionic TO-CNF and S-CNF as a shell was tested. It was rapidly detected that these filaments broke easily and were difficult to lift to the winder. When components were reversed opposite, so that TO-CNF and S-CNF were on the core and CDAC-CNF in the shell, filaments did not break that easily and were able to be lifted on the winder immediately. This could be explained by ionic crosslinking phenomenon of anionic CNFs. When TO-CNF is wet-spun using $CaCl_2$ as a coagulant, ionic crosslinks are created between carboxylic acid groups of TO-CNFs (Kafy et al. 2017). Additionally, oppositely charged core and shell are interacting via interfacial complexation. When cationic CNF was on the core and anionic in the shell, the ionic crosslinking mediated by Ca^{2+} was prevented, and the interfacial complexation didn't provide enough strong adhesion between the CNFs to obtain continuous filaments. In case of TO-CNF/CDAC-CNF and S-CNF/CDAC-CNF, Ca^{2+} crosslinked TO-CNF and S-CNF, thus gelation occurred, and filaments were strong enough to be lifted from coagulant.

SC-CNF was infeasible for filament production, because water was separated from CNF during centrifugation but also in tube between syringe pump and needle during extrusion. This was most probably due to too low surface charge of SC-CNF. High surface charge promotes stronger and more stable CNF, and enhances the hydrogel stability. (Mendoza et al. 2018)

Filament shrinking during coagulation was observed, especially for S-CNF/CDAC-CNF. Comparing S-CNF/CDAC-CNF and TO-CNF/CDAC-CNF fabricated with same spinning speed, drawing speed of S-CNF/CDAC-CNF was lower, but resulted approximately same widths of the filaments than TO-CNF/CDCA-CNF (Table 3, Appendix 2).

Weak wet strength of the filaments, that caused filament breaking, was challenging for continuous processing. Different positions for drying and winding were tested to discover suitable apparatus, which made it possible to produce unbroken filaments. Winder was placed on a podium, flipped sideways and set slightly above the coagulation bath. It was also observed that roller between coagulation sink and winder was essential to support low wet strength filaments, and to prevent filaments from breaking, and help drying.

Fabrication of S-CNF/CDAC-CNF was more problematic compared to TO-CNF/CDAC-CNF since these filaments were more prone to break. Additionally, core and shell layers tend to separate from each other occasionally. This may be explained by a lower CNF solids content (1.6 wt%) in S-CNF/CDAC-CNF than that of TO-CNF/CDAC-CNF (1.8 wt% and 1.9 wt%). Solid content of CNF close to 2 wt% resulted in stronger filaments than solid content of 1 wt% (Lundahl et al. 2016). Additionally, differences in charge density could be the reason. Difference between negative and positive charge is lower for TO-CNF/CDAC-CNF compared to S-CNF/CDAC-CNF (Table 1), which could allow better interaction between CNFs.

In addition to oppositely charged CNF pairs, filaments containing TO-CNF only, i.e. TO-CNF/TO-CNF, were also produced. However, there were many difficulties in the spinning process. Stretching of TO-CNF/TO-CNF was more difficult due to its sensitivity to break. Thus, drawing speeds for TO-CNF/TO-CNF were lower, and filaments were slightly wider than other filaments (shown in Table 3, Appendix 2). Filaments were also adhered on the Teflon roller located between coagulation bath and winder, thus causing

twitching of filaments, that may have affected the properties of filaments. Presumably this was because of scuffed roller. Sticking was reduced by covering roller with Teflon spray but as surface wore out, filaments stuck the tube again. Interaction of TO-CNF/TO-CNF is assumed to be slower than TO-CNF/CDAC-CNF and S-CNF/CDAC-CNF, which were formed by interfacial complexation. For TO-CNF/TO-CNF cross-linking occurring during coagulation is the only driving force for filament formation. For core-shell filaments interfacial complexation together with cross-linking caused the filament formation. Higher interaction and adhesion of CNFs might result in higher wet-strength of TO-CNF/CDAC-CNF and S-CNF/CDAC-CNF. Lower wet-strength of TO-CNF/TO-CNF could lead to its tendency to break.

4.3 Characterization of fabricated filaments

Both TO-CNF/CDAC-CNF and S-CNF/CDAC-CNF had a slightly yellowish colour (Figure 13), which was most likely due to a bit yellow appearance of CDAC-CNF and S-CNF. Optical microscopy images of filaments are shown in Figure 15. All filaments had dense structure and most of them were flexible enough to form a knot (Figure 15a). Only washed filaments and TO-CNF/CDAC-CNF fabricated at spinning speed ratio of 1/1.5 were not able to form unbroken knot, thus they exhibited more rigid structure.

Along the filament axis, veining patterns were also detected, especially in S-CNF/CDAC-CNF and TO-CNF/TO-CNF (Figure 15c). Rather similar veining patterns were previously observed for filaments fabricated using interfacial complexation (Zhang and Liimatainen 2018). Veining indicates alignment along the filament axis. The longitudinal structure of TO-CNF/CDAC-CNF is coarser and veining patterns are less visible compared to S-CNF/CDAC-CNF and TO-CNF/CDAC-CNF (Figure 15c) exhibiting poorer CNF orientation.

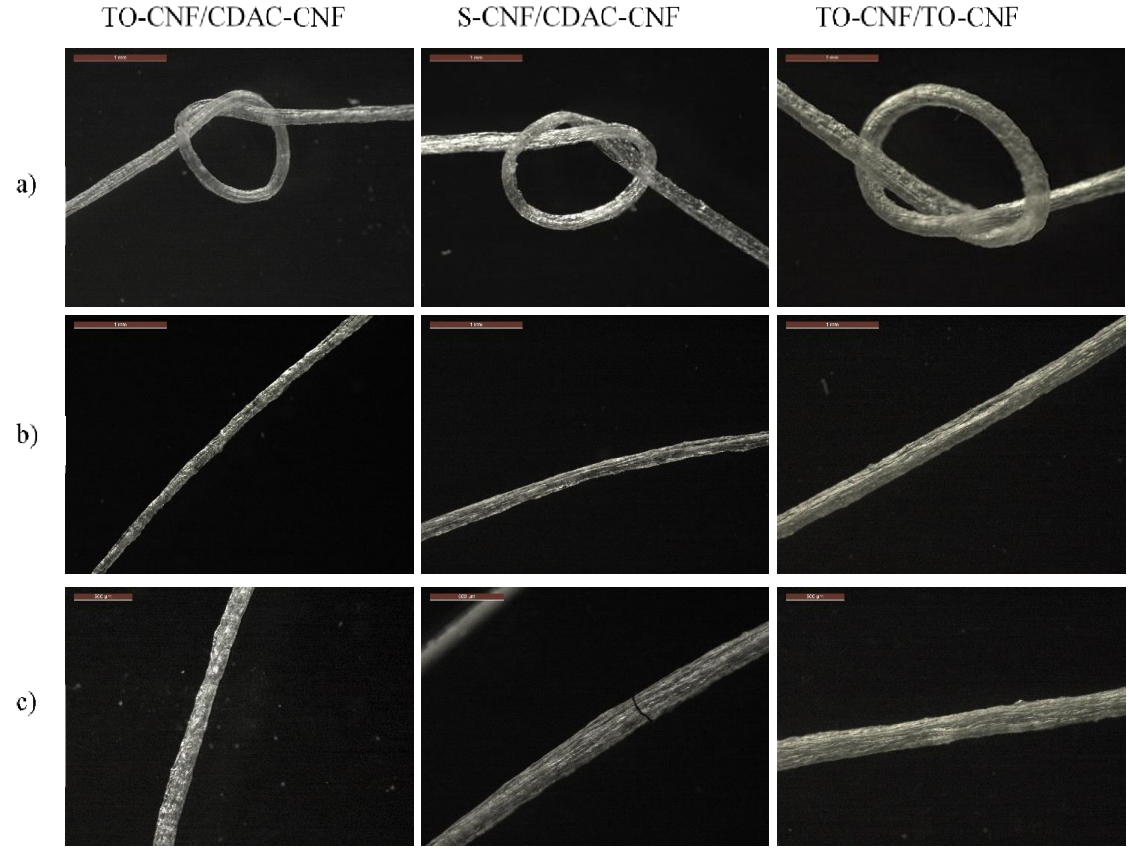

Figure 15. Optical microscopy images of fabricated filaments.

Figure 16. displays the effect of the stretching on filament appearance. More stretched filament with a smaller width (Figure 16b) had a dense structure and more visible veining patters along the axis comparing to less stretched filament (Figure 16a). This indicates better CNF alignment in the filament due to stretching.

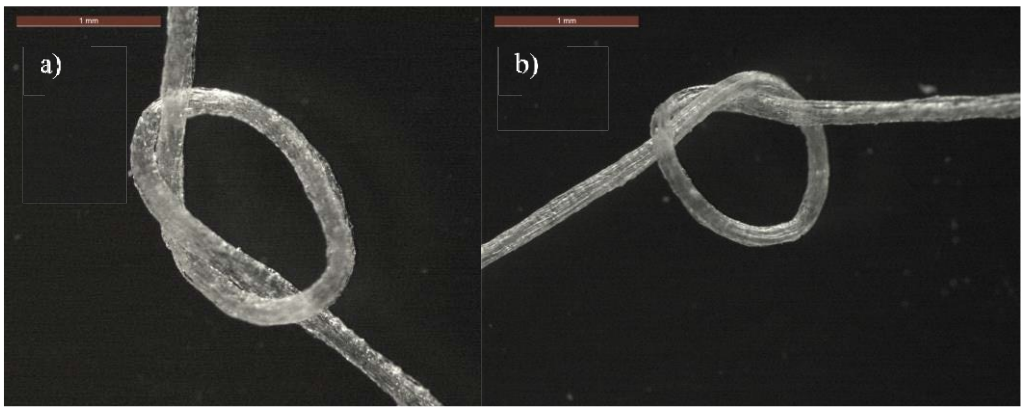

Figure 16. TO-CNF/CDAC-CNF fabricated at a) 0.250 mL/min with the filament width of 210 µm mm and b) 0.550 mL/min with the filament width of 140 µm.

Figure 17 presents some inhomogeneities along filaments axis, which are probably undesirable to the mechanical properties of the filaments. Short fibers, pulled out from the filament, were observed on the surface of all the filaments (Figure 17a), but the most on TO-CNF/TO-CNF filaments, which had thick, long and aggregated fibers on the surface (Figure 17b). This indicates poor interaction and adhesion between the CNFs and may have affected the mechanical properties of the filaments. Additionally, longitudinal axis of TO-CNF/TO-CNF contained many bubbles (Figure 17c), which could be the result of residual air in TO-CNF. TO-CNF/TO-CNF consisted of only TO-CNF, which was less viscose and contained more air, compared to CDAC-CNF, that was used as a core in other filaments. Most of these bubbles were clearly visible, and these parts of the filaments were not included in the mechanical tests.

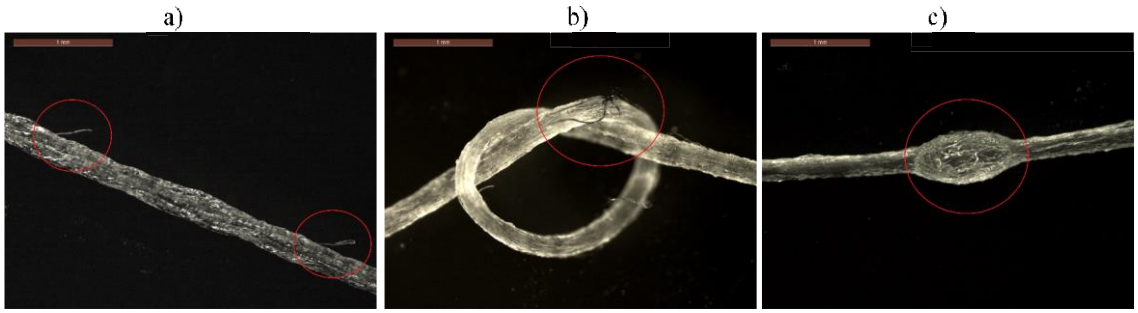

Figure 17. Optical microscopy images of inhomogeneous areas along filament axis; a) pulled out fibers on the surface of S-CNF/CDAC-CNF and b) TO-CNF/TO-CNF, and bubbly assembly along TO-CNF/TO-CNF axis.

Flattening of the filaments on the winder was reduced by both drying filaments before winder but also by covering winder with Teflon spray. There was significant difference between flattened and less flattened filaments (Figure 18). However, flattening could not be completely avoided.

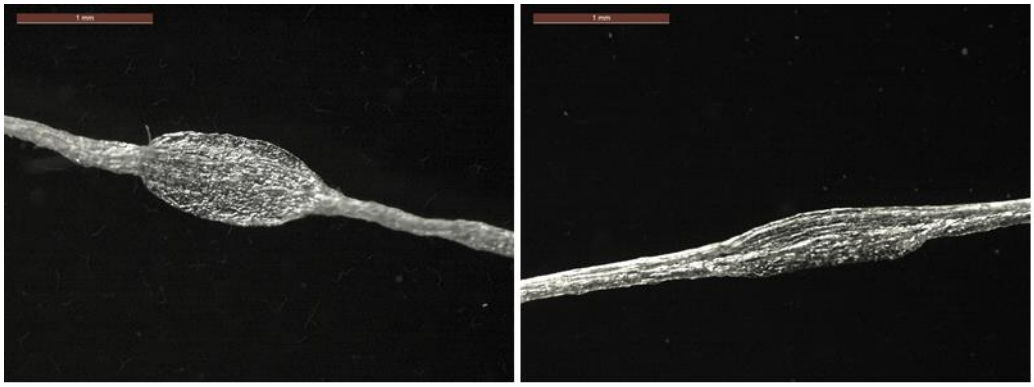

Figure 18. Largely (left) and less (right) flattened filaments.

Cross-sectional areas of filaments are shown in Figure 19. The cross-sections of the fabricated filaments were irregular circles and displayed coarse longitudinal surface. (Figure 19a-b). This could be due to coagulation process. Cross-sectional shape of the filament is determined by difference of mass transfer rate of water in CNF and coagulant solution. If the mass transfer rate of water is higher than that of the coagulant, filaments shrink in the bath and noncircular cross-section is beneficial (Wang et al. 2019). This was observed during filament production, especially for S-CNF/CDAC-CNF, thus could explain the irregular cross-section of the filaments, and use of other coagulant could result in smoother filaments. Interestingly, cross-section of TO-CNF/TO-CNF is also irregular. TO-CNF filament should swell during coagulation in $CaCl_2$ and circular cross section should be favoured (Wang et al. 2019). Previously fabricated filaments using interfacial complexation and wet spinning (TO-CNF filaments coagulated in $CaCl_2$) presented smoother longitudinal surface and circular cross-section (Zhang and Liimatainen 2018; Kafy et al. 2017; Kim et al. 2019; Wang et al. 2019). However, filaments fabricated in this study, presented homogenous cross-section without clear interface between the core and shell. It is assumed that core and shell were partially mixed, and this phenomenon was facilitated by interfacial complexation of CNFs. Previously, fabricated core-shell filaments cross-sections exhibited visible interface between core and shell (Reyes et al. 2020).

Some aligned layers can be detected in TO-CNF/CDAC-CNF and especially in TO-CNF/TO-CNF at high magnification (Figure 19c). TO-CNF/TO-CNF, and partly TO-CNF/CDAC-CNF, have a foliaceous network, which exposes better orientation of CNF comparing to S-CNF/CDAC-CNF, in which cross-sectional surface is rather smooth, and

fibers are presumably transversely. This indicates negligible fiber orientation of S-CNF/CDAC-CNF. However, compared to previous studies, structure of TO-CNF/TO-CNF is also related to poor orientation of CNF since appearance of layer network is slightly undirected and undulated. Similar structure was previously reported for unstretched i.e., poorly oriented TO-CNF filaments (Torres-Rendon et al. 2014).

On the surface and/or inside of the filaments, lots of spherical particles were clearly detected (Figure 19d), which were assumed to be formed from the excess of coagulant salt. Sal was observed inside and on the surface of TO-CNF/CDAC-CNF, and inside of S-CNF/CDAC-CNF and TO-CNF/TO-CNF. $CaCl_2$ facilitate CNF coagulation through ion exchange. During coagulation calcium cations diffuse in TO-CNF and replace Na+ (Wang et al. 2019), thus presence of calcium in filament indicates successful ion exchange between Ca^{2+} and Na^{+}, resulting in improved ion interaction and hydrogen bonding between CNFs (Kim et al. 2019). Even if ion exchange improves ion interaction, presence of residual salts may have an impact on the mechanical properties.

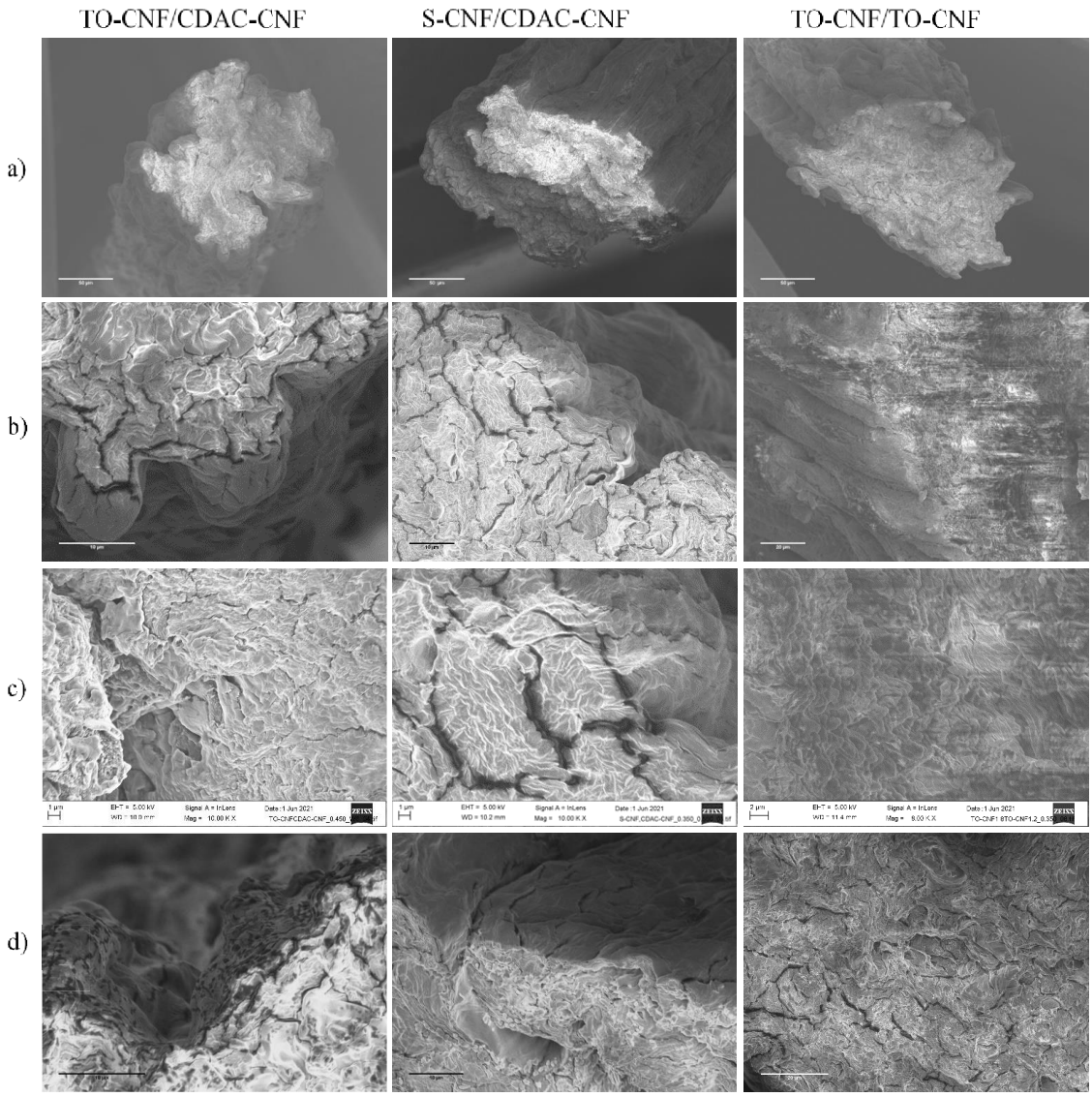

Figure 19. FESEM images of cross-sectional areas of fabricated filaments.

4.4 Mechanical properties of fabricated filaments

Mechanical properties of filaments, in terms of tensile strength, Young's modulus and strain at tensile strength, were investigated. In place of strain at break, strain at tensile strength was used since tensile test machine displayed only this value. In this work strain at tensile strength is estimated to be close to the value of strain at break, thus comparable to the previous studies in which strain at break is presented. Fabricated filaments, their mechanical properties and widths are shown in Table 3, Appendix 2.

4.4.1 The effect of drying temperature on mechanical properties

The effect of drying temperature on the mechanical properties of the fabricated filaments was investigated and TO-CNF/CDAC-CNF, S-CNF/CDAC-CNF and TO-CNF/TO-CNF were dried at five different temperatures (450, 500, 550, 600, and 650 °C). The mechanical properties of the filaments are shown in Figure 20. At a drying temperature of 450 °C, the tensile strength, Young's modulus, and strain were around 5.3 MPa, 341 MPa and 1.9 % for TO-CNF/CDAC-CNF, 5.3 MPa, 181 MPa and 3.8 % for S-CNF/CDAC-CNF, and 7.5 MPa, 19 MPa and 21 % for TO-CNF/TO-CNF, respectively. When the temperature increased to 500 °C, minor increase in tensile strength and Young's modulus were detected for TO-CNF/CDAC-CNF and S-CNF/CDAC-CNF. Meanwhile, major increase in tensile strength and Young's modulus for TO-CNF/TO-CNF was observed. Tensile strength rose to a maximum value of 8.2 and 13.5 MPa at a drying temperature of 500 °C for TO-CNF/CDAC-CNF and TO-CNF/TO-CNF, respectively, and 7.1 MPa at 550 °C for S-CNF/CDAC-CNF. Similarly, Young's modulus of TO-CNF/CDAC-CNF reached the maximum value of 577 MPa at 500 °C and S-CNF/CDAC-CNF of 260 MPa at 550 °C. With further increase in drying temperature, tensile strength and Young's modulus decreased. This might be explained by hydrogen bonding occurring during drying. At high temperatures, interchain hydrogen bonds in cellulose dominate, which result in agglomeration of CNFs, thus decreasing the strength of the filament (Agarwal et al. 2011, Peng et al. 2012). However, as drying temperature increased, Young's modulus for TO-CNF/TO-CNF increased reaching maximum value of 153 MPa at 650 °C, which is nevertheless lower than highest values of TO-CNF/CDAC-CNF and S-CNF/CDAC-CNF.

As temperature increased, only slight change in strain for TO-CNF/CDAC-CNF (around 2 %) and S-CNF/CDAC-CNF (around 4 %) occurred. Oppositely, strain for TO-CNF/TO-CNF significantly decreased as temperature increased. Strain for TO-CNF/TO-CNF reached maximum value of 21 % at 450 °C, which was significantly higher than of TO-CNF/CDAC-CNF and S-CNF/CDAC-CNF at any temperature. Decrease in strain could refer to a stronger hydrogen bonding as drying temperature increased. Simultaneous increase in Young's modulus support this argument.

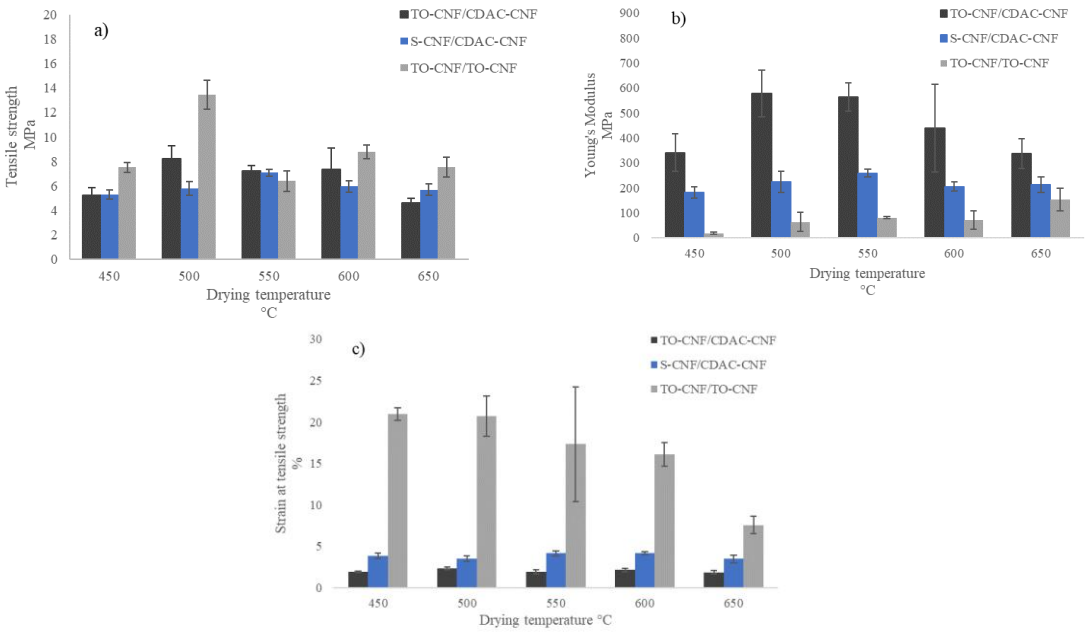

Figure 20. Mechanical properties of filaments in terms of a) tensile strength, b) Young's modulus and c) strain as a function of drying temperature.

4.4.2 The effect of spinning speed on mechanical properties

The effect of spinning speed on the mechanical properties of the fabricated filaments was investigated and TO-CNF/CDAC-CNF, S-CNF/CDAC-CNF and TO-CNF/TO-CNF were fabricated at different speeds (0.250, 0.350, 0.450, 0.550). The mechanical properties of the filaments are shown in Figure 21. At spinning speed of 0.250 mL/min, the tensile strength, Young's modulus, and strain were around 4.6 MPa, 220 MPa and 2.5 % for TO-CNF/CDAC-CNF; 2.5 MPa, 19MPa and 20 % for S-CNF/CDAC-CNF; and 6 MPa, 24 MPa and 20 % for TO-CNF/TO-CNF, respectively. When the spinning speed increased, tensile strength for TO-CNF/CDAC-CNF and TO-CNF/TO-CNF increased reaching maximum values of 11 MPa at 0.550 mL/min for TO-CNF/CDAC-CNF, and 18 MPa at 0.450 mL/min for TO-CNF/TO-CNF. S-CNF/CDAC-CNF reached its maximum value of 5.7 MPa at 0.350, after which tensile strength decreased as spinning speed increased. Young's modulus for TO-CNF/CDAC-CNF increased as spinning speed increased reaching maximum value of 786 MPa at 0.550 mL/min. Young's modulus for S-CNF/CDAC-CNF and TO-CNF/TO-CNF increased as spinning speed increased from 0.250 mL/min to 0.350 mL/min, after which values decreased. Highest values were 213 MPa for S-CNF/CDAC-CNF and 153 MPa for TO-CNF/TO-CNF. Strain at tensile

strength remained at the same level, close to 20 % for S-CNF/CDAC-CNF and TO-CNF/TO-CNF, and 2 % for TO-CNF/CDAC-CNF, apart from spinning speed of 0.350 mL/min, that was significantly lower for S-CNF/CDAC-CNF and TO-CNF/TO-CNF.

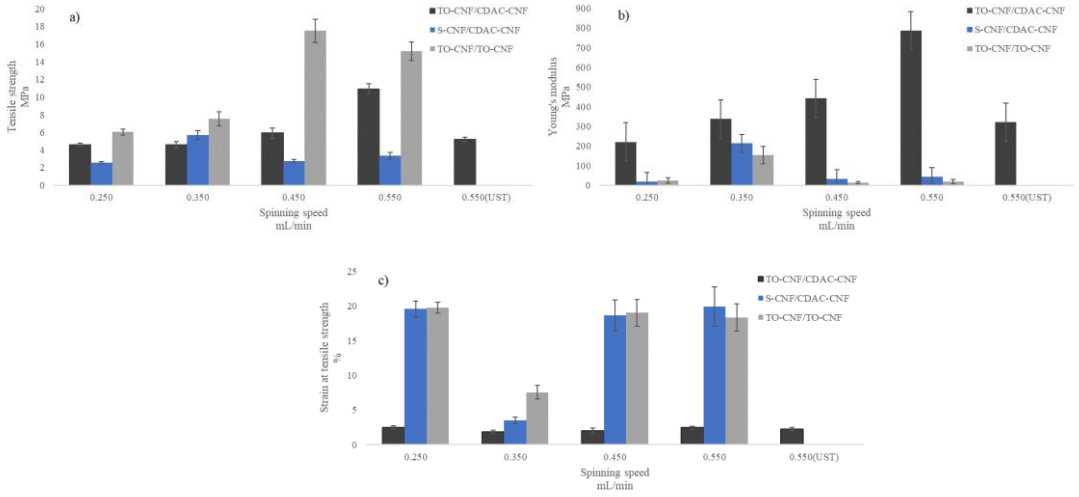

Figure 21. Mechanical properties of filaments in terms of a) tensile strength, b) Young's modulus and c) strain as a function spinning speed.

For comparison, unstretched TO-CNF/CDAC-CNF (UST in Figure 21) was fabricated at spinning speed of 0.550 mL/min. Stretching seemed to be the main reason for increasing tensile strength and Young's modulus as spinning speed increased, since those values notable dropped for unstretched filament. However, tensile strength and Young's modulus were slightly higher for unstretched filament fabricated at 0.550 mL/min than stretched filament fabricated at 0.250 mL/min. This showed that increased spinning speed had a minor effect on mechanical properties. However, stretching was the main reason for improvement in tensile strength and Young's modulus. Similarly, for S-CNF/CDAC-CNF increase in tensile strength and Young's modulus and decrease in strain at spinning speed of 0.350 mL/min can be explained by stretching. This filament was stretched most, thus width was the smallest (Table 3, Appendix 2). The effect of stretching is more closely discussed in the section 4.4.5.

Additionally, the effect of spinning speed was investigated so that speed of shell was higher than core. TO-CNF/CDAC-CNF, S-CNF/CDAC-CNF and TO-CNF/TO-CNF were fabricated so that spinning speed of shell was 20, 50, and 70 % higher than core. Spinning speed of core was kept constant, for TO-CNF/CDAC-CNF and TO-CNF/TO-

CNF it was 0.350 mL/min, while 0.450 mL/min for S-CNF/CDAC-CNF. Higher spinning speed was selected for S-CNF/CDAC-CNF because lower speed was unpredictable, and core and shell tend to separate from each other in coagulation bath or shell teared from the core on roller. Increase in spinning speed in core was notably better for filament fabrication.

The mechanical properties of filaments are shown in Figure 22. When spinning speed of shell was 20 and 50 % higher than core, tensile strength and Young's modulus of TO-CNF/CDAC-CNF and S-CNF/CDAC-CNF increased. Maximum values for tensile strength and Young's modulus of 8.2 MPa and 676 MPa for TO-CNF/CDAC-CNF, and 6 MPa and 78 MPa for S-CNF/CDAC-CNF, respectively, were reached when spinning speed ratio was 1/1.2. Slight change in values was observed as ratio increased to 1/1.5. With further increase of spinning speed to 70 %, tensile strength and Young's modulus decreased. Interestingly, width of the filaments were related to spinning speed. When spinning speed of core increased 20 and 50 %, filaments became thinner even if drawing speed was constant. (Table 3, Appendix 2) Further increase in spinning speed produced broader filaments. This might be explained by better CNF orientation in the filaments. As increasing the spinning speed in the shell, shear forces inside the needle (shell) improve the alignment of CNFs and nanofibers were packed tighter in filament, that was shown in smaller width of the filaments. However, with further increase in spinning speed, orientation declined due to uncontrolled shear forces that caused unoriented nanofibers, thus increased filament width and decreased mechanical properties. Similar effect of spinning speed on mechanical properties has been demonstrated by Kim et al. (2019). Strain of TO-CNF/CDAC-CFN was around 2 % apart from spinning speed, whereas of S-CNF/CDAC-CNF slight change was observer when speed increased to 1/1.2 when reached maximum value of 24 %. Further increase slightly decreased the strain.

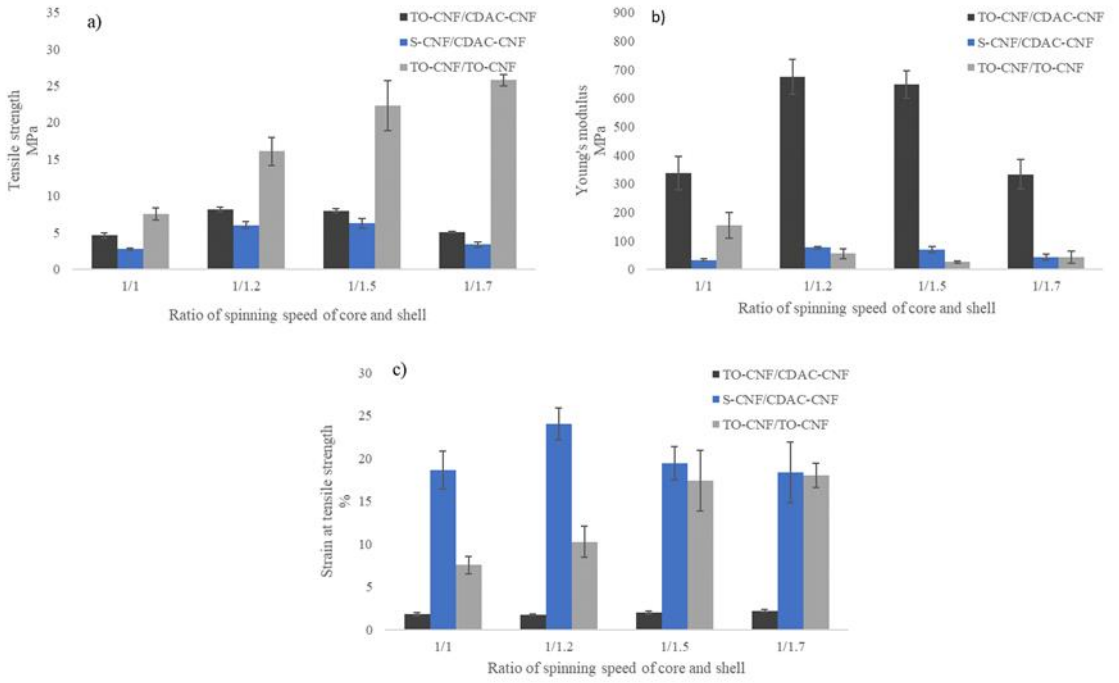

Figure 22. Mechanical properties of filaments in terms of a) tensile strength, b) Young's modulus and c) strain as a function of spinning speed ratio of core/shell.

In case of TO-CNF/TO-CNF, filaments behaved differently compared to TO-CNF/CDAC-CNF and S-CNF/CDAC-CNF. When spinning speed of shell increased, tensile strength and strain increased but Young's modulus decreased. Decreased Young's modulus was a result of weaker hydrogen bonding due to higher speed. An internal adhesion of TO-CNF/TO-CNF is lower than oppositely charged TO-CNF/CDAC-CNF and S-CNF/CDAC-CNF. Weaker hydrogen bonding is also a result for strain increase. Tensile strength and strain reached maximum values of 26 MPa and 18 %, respectively, with 70 % higher spinning speed of shell. Tensile strength is also significantly higher than that value for TO-CNF/CDAC-CNF and S-CNF/CDAC-CNF, meanwhile strain is close to S-CNF/CDAC-CNF. Young's modulus reached maximum value of 153 MPa when spinning speed of core and shell were equal. Difference between TO-CNF/TO-CNF and other filaments could be explained by the different mechanism of filament formation. Interfacial complexation method was utilized for formation of S-CNF/CDAC-CNF and TO-CNF/CDAC-CNF. Too high spinning speed decrease interaction time between oppositely charged CNFs thus can decrease tensile strength and Young's modulus. Higher spinning speed is advantageous for tensile strength of TO-CNF/TO-CNF since there is

no need for interaction. However, high speed result in weaker hydrogen bonding thus lower Young's modulus.

4.4.3 The effect of needle size on mechanical properties

The effect of needle size on mechanical properties was investigated using two different needles. Additionally, spinning speed of core was increased to study potential effect of it. The mechanical properties are shown in Figure 23. For TO-CNF/CDAC-CNF, needle change from bigger (20/16G) to smaller (22/18G) was largely disadvantageous since tensile strength and Young's modulus significantly decreased at the most of the spinning speeds. Solely, tensile strength at 1/1 ratio of spinning speed remained unchanged. Decrease in tensile strength and Young's modulus is most likely due to too high shear rate that forces nanofibers to curl thus leading to poor alignment of CNF (Rosen et al. 2020b). Strain at tensile strength increased using smaller needle. With other parametres strain was unchanged 2 %, but with smaller needle increased to around 10 %. Increased strain additionally refers to poorer orientation of nanofibers in filaments. Increasing spinning speed with smaller needle seemed not to have an effect on mechanical properties, since values remained around the same levels; tensile strength around 4 MPa, Young's modulus around 150 MPa, and strain around 10 %.

For S-CNF/CDAC-CNF Young's modulus slightly increased with smaller needle. Tensile strenght and strain alternated being higher or lower depending on the ratio of spinning speed, thus it is difficult to draw clear conclusions of the effect of needle size. However comparing to TO-CNF/CDAC-CNF, smaller needle can be advantageous for S-CNF/CDAC-CNF. For example, at spinning speed ratio of 1/1.7 for core and shell, tensile strength, Young's modulus and strain increased from 3.4 to 4.9 MPa, from 42 to 120 MPa, and from 18 to 21 %, respectively. However, tensile strength is lower than what was reached with lower spinning speed and bigger needle.

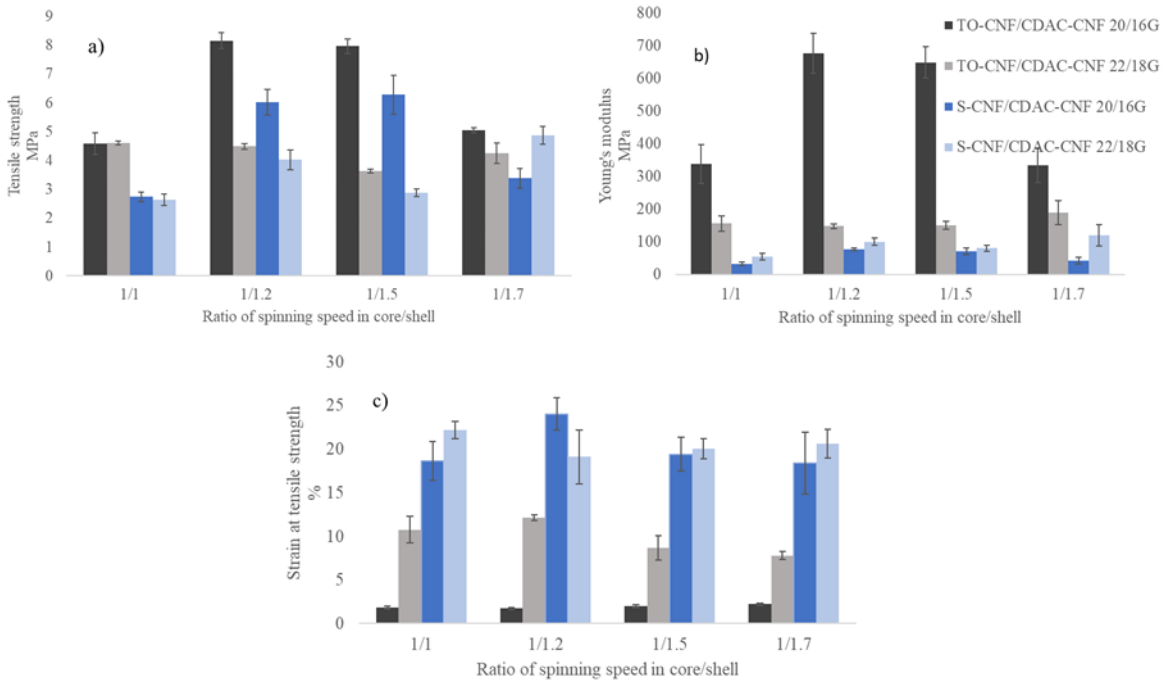

Figure 23. Mechanical properties of filaments fabricated with different needles in terms of a) tensile strength, b) Young's modulus and c) strain as a function of spinning speed ratio of core/shell.

4.4.4 The effect of washing on mechanical properties

The effect of washing was investigated by immersing TO-CNF/CDAC-CNF, S-CNF/CDAC-CNF and TO-CNF/TO-CNF into water for 24 h, followed by drying at 650 °C. Filaments, that were fabricated with spinning speed 20 % higher in shell feeding velocity were selected for washing, since they had good mechanical properties according to previous tests. Structure of washed filaments was curly, coarser and stiffer than corresponding unwashed filaments and were not flexible enough to tie a knot (Figure 26, Appendix 3). For TO-CNF/CDAC-CNF width of the filament decreased from 158 to 139 µm, and for S-CNF/CDAC-CNF from 181 to 152 µm but increased for TO-CNF/TO-CNF from 186 to 200 µm (Table 3, Appendix 2).

The mechanical properties of the filaments are shown in Figure 24. Washing significantly increased tensile strength of the filaments. Tensile strength increased from 8 to 67 MPa for TO-CNF/CDAC-CNF, from 6 to 105 MPa for S-CNF/CDAC-CNF, and from 16 to 78 MPa for TO-CNF/TO-CNF. Presence of calcium ions, shown in FESEM-images, is probably the main reason for lower tensile strength of unwashed filaments. According to previous studies washing removes the excess salts from filaments (Wang et al. 2019),

densifies the filaments and washed filaments displayed higher tensile strength and Young's modulus but lower strain (Reyes et al 2020). Washing increased tensile strengths, especially for TO-CNF/CDAC-CNF, closer to values previously reached (153 MPa and 172 MPa) for nanocellulose-based filaments formed via interfacial complexation and coaxial wet spinning but was still significantly lower (Zhang and Liimatainen 2018; Reyes et al. 2020).

However, washing decreased Young's modulus. Young's modulus of TO-CNF/CDAC-CNF drop from 675 MPa to 115 MPa, while a decrease of S-CNF/CDAC-CNF and TO-CNF/TO-CNF were more moderate since their initial Young's modulus's were under 100 MPa. This could be result of CNF relaxation during 24 h washing as water diffuse in the filaments, thus caused disordered nanofiber orientation. After washing, strain slightly decreased for S-CNF/CDAC-CNF and TO-CNF/TO-CNF but increased for TO-CNF/CDAC-CNF. Decrease in strain after washing was expected based on previous studies. Increased strain of TO-CNF/CDAC-CNF can be assumed to be unreliable result.

It must consider that washing was performed afterwards for 24 h, thus circumstances were different than if washing would be connected directly to continuous process. For appropriate filament fabrication process, washing must be included in the process.

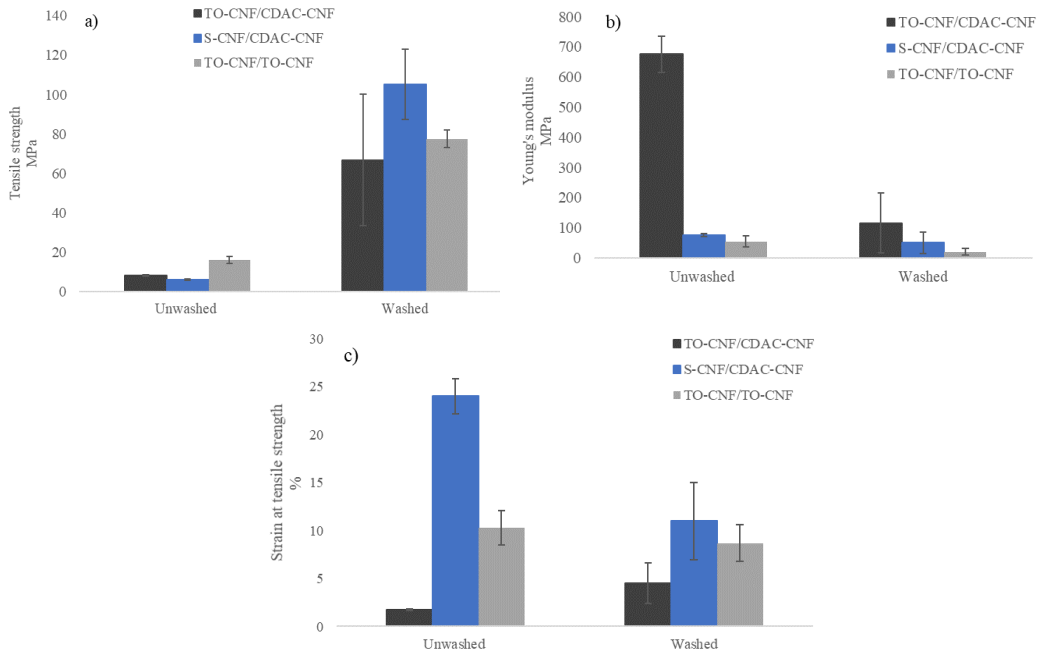

Figure 24. The effect of washing on mechanical properties in terms of a) tensile strength, b) Young's modulus and c) strain for washed and unwashed filaments.

4.4.5 The effect of stretching on mechanical properties

As mentioned earlier, stretching showed to be an important parameter to increase tensile strength and Young's modulus of filaments. Stretching decreased width of the filaments. Width ranged from 132 µm to 213 µm for TO-CNF/CDAC-CNF, from 138 µm to 265 µm for S-CNF/DAC-CNF, and from 183 µm to 308 µm for TO-CNF/TO-CNF (Table 3, Appendix 2) depending on how stretching succeeded. Compared to previous results of Zhang and Liimatainen (2018) width of the filaments prepared in this study are notably larger. Reyes et al. (2020) used approximately same sized coaxial needle as in this study, and width of filaments were similar.

The effect of stretching was investigated by means of drawing ratio. The DRs between drawing speed and spinning speed are shown in Table 3 in Appendix 2. Note that most of the DRs were under 1 even if stretching was occurring. This was due to shrinking in coagulation bath, thus drawing speed of the winder was mainly slower than spinning speed. Figure 25 shows the mechanical properties of filaments as a function of drawing ratio. As stretching increased (greater DR of filaments), tensile strength of TO-CNF/CDAC-CNF and TO-CNF/TO-CNF increased, whereas S-CNF/CDAC-CNF slightly decreased. Note the highlighted washed filaments, that had the highest tensile strengths, which affect especially to trendline of S-CNF/CDAC-CNF. Simultaneously, Young's modulus of TO-CNF/CDAC-CNF and S-CNF/CDAC-CNF increased. For TO-CNF/TO-CNF increasing stretching slightly decreased Young's modulus. Strain of all the filaments decreased as drawing ratio increased. Improvement in tensile strength and Young's modulus and impairment in strain by stretching is a result of better nanofiber orientation. Similar effect was previously attained using TO-CNF for filament production (Torres-Rendon et al. 2014; Kafy et al. 2017).

Additionally, overall trend between filaments mechanical properties can be seen in Figure 25. Highest DR values were attained for TO-CNF/CDAC-CNF, which was easiest to be stretched. Increasing trend for tensile strength was highest for TO-CNF/TO-CNF, even with low DRs. TO-CNF/CDAC-CNF and S-CNF/CDAC-CNF are rather close to each other in terms of tensile strength. Oppositely, Young's modulus was highest for TO-CNF/CDAC-CNF and lowest for TO-CNF/TO-CNF. Thus TO-CNF/TO-CNF seemed to be best oriented in terms of tensile strength, but Young's modulus was lowest showing poor hydrogen bonding.

Strains of S-CNF/CDAC-CNF and TO-CNF/TO-CNF were significantly higher than of TO-CNF/CDAC-CNF. Typical stress-strain curves of fabricated filaments (Figure 25d) additionally showed that TO-CNF/CDAC-CNF and TO-CNF/TO-CNF are stiffer than S-CNF/CDAC-CNF. This can be explained by different CNFs. Filaments spinnability and capability to be stretched correlates with DP of cellulose; high DP causes stronger and stiffer filaments (Michud et al. 2015; Lundahl et al 2017). DP of cellulose decreases during sulfation (Sirviö et al. 2019), which is assumed to be the reason for flexibility of S-CNF/CDAC-CNF.

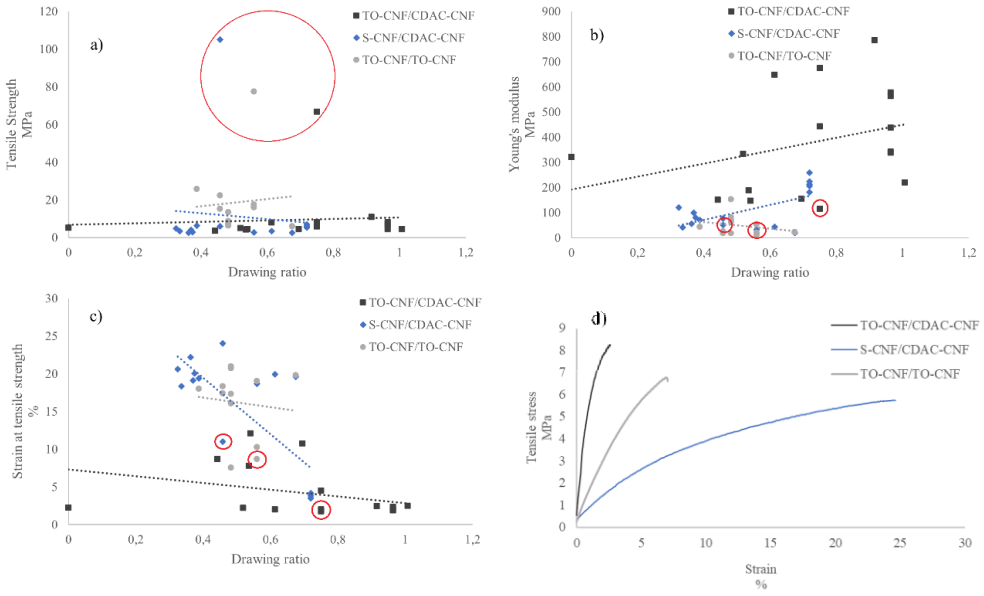

Figure 25. The mechanical properties of filaments as a function filament drawing ration in terms of a) tensile strength, b) Young's modulus and c) strain, and d) typical stress-strain curves of fabricated filaments. Washed filaments are highlighted.

5 CONCLUSIONS

In this study, continuous fabrication process was successfully developed for core-shell filament production from cellulose nanofibers. Interfacial complexation and wet spinning were combined with drying step and filaments were collected on a winder. CNF with anionic charge as a core and cationic charge as a shell was shown to be only suitable structure for continuous filament fabrication, thus filaments consisting of TO-CNF/CDAC-CNF, S-CNF/CDAC, and TO-CNF/TO-CNF were successfully fabricated. Additionally, air removal from CNF suspensions and minimum friction of the filament during processing were requirements that prevented filament from breaking and enabled a continuous process.

Fabrication of S-CNF/CDAC-CNF was more uncertain comparing to TO-CNF/CDAC-CNF, which was assumed to be due to lower consistency and poorer interaction between CNFs. Structure of TO-CNF/CDAC-CNF and S-CNF/CDAC-CNF was rather similar. Veining along longitudinal axis was shown, but cross-sectional images showed few oriented nanofibers. Based on cross-sectional images, TO-CNF/TO-CNF had the highest degree of oriented nanofibers. On the other hand, there were lots of aggregated fibers pulled out from the TO-CNF/TO-CNF longitudinal axis and problems during its fabrication. Signs of orientation, such as structure tightening due the stretching, and axial veining was shown along all filaments' axes. However, comparing to previous studies, filaments were poorer oriented, which was probably the cause for low mechanical properties.

Process parameters were optimized by means of drying temperature, spinning speed, needle size and washing. Stretching was shown to be important parameter in terms of filaments mechanical properties. For drying temperature, spinning speed and needle size optimal condition were found. Drying temperature around 500 - 550 °C, spinning speed ratios of 1/1.2 and 1/1.5 for core-shell and bigger needle (20/16G) were the most advantageous for TO-CNF/CDAC-CNF and S-CNF/CDAC-CNF. Long enough time for interaction between CNFs was shown to has an effect on mechanical properties. For TO-CNF/CDAC-CNF the highest tensile strength and Young's modulus were 11 MPa and 787 MPa, respectively, whereas for S-CNF/CDAC-CNF 7.1 MPa and 260 MPa, respectively.

For TO-CNF/TO-CNF tensile strength and Young's modulus were not consistent. Roughly speaking, when tensile strength increased Young's modulus decreased. Highest value of tensile strength (25 MPa) was achieved when 1/1.7 ratio of core/shell spinning speed was used. Young's modulus was highest (153 MPa) with 650 °C drying temperature and 0.350 mL/min spinning speed. Problems during spinning with TO-CNF/TO-CNF can have affected to contradictory result.

Washing was not attached to the experimental process, but the effect of washing was investigated afterwards. Washing significantly increased tensile strength and highest values of 67 MPa for TO-CNF/CDAC-CNF, 105 MPa for S-CNF/CDAC-CNF, and 78 MPa for TO-CNF/TO-CNF were reached. Contradictory, washing decreased Young's modulus, which was assumed to be due to long washing time that caused nanofiber relaxation and resulted in disordered nanofiber orientation. Mainly reached tensile strengths in this study were remarkable lower than previously reported strengths achieved using interfacial complexation or traditional wet spinning (Zhang and Liimatainen 2018; Kim et al. 2019). Washing improved notably tensile strengths but they were still lower. Young's modulus's were even 100 times lower comparing to previous studies. However, highest strain of 24 % for S-CNF/CDAC-CNF was around three times higher than previously reported for interfacial complexation and significantly higher than the best reported values in wet spinning. Flexibility of S-CNF/CDAC-CNF could be advantageous for some applications, such as electronics.

When compared TO-CNF/TO-CNF to core-shell filaments, results were positive. Even if tensile strength was mostly highest for TO-CNF/TO-CNF, mechanical properties of TO-CNF/CDAC-CNF and S-CNF/CDAC-CNF were rather close to it on a large scale. Additionally, highest tensile strength was reached for washed S-CNF/CDAC-CNF. This means that, core-shell filaments can be considered comparable to TO-CNF/TO-CNF, even if strength properties were lower than previously reported. Additionally, S-CNF/CDAC-CNF was purely based on DES CNF. It could be concluded that core-shell filament fabricated using only DES treated CNF showed similar or even better (washed S-CNF/CDAC-CNF) properties as TO-CNF/CDAC-CNF and TO-CNF/TO-CNF. Thus, greener DES based filament was shown to have potential in filament fabrication.

More investigations are still needed for a feasible continuous production of stronger and better structured core-shell filaments, but potential of TO-CNF/CDAC-CNF and S-CNF/CDAC-CNF have been proved during this research. Additionally, the attachment of washing to the continuous process is necessity for better mechanical properties of filaments. It is assumed that faster (than 24 h) washing right after coagulation would also increase Young's modulus, which was now decreased. Controlling of stretching is also important element for further studies regarding to continuous filament fabrication, since it was shown to be extremely important for nanofiber orientation and mechanical properties.

6 SUMMARY

In this study, continuous process for core-shell filament production was developed in laboratory scale by utilizing interfacial complexation and wet spinning of cellulose nanofibers. The literature part consisted of the description of cellulose nanomaterials and their production methods, cellulose filaments, their spinning methods and parameters related to spinning. In the experimental part, a continuous spinning process was developed by interconnecting different process steps, i.e. CNF extrusion through coaxial spinneret, coagulation, drying and winding. Different core-shell filaments, TO-CNF/CDAC-CNF, S-CNF/CDAC-CNF and TO-CNF/TO-CNF as a reference were produced and process was optimized by investigating different process parameters such as spinning speed, drying temperature, stretching, needle size and washing. The filaments were evaluated by microscopy imaging and tensile strength tests.

The main findings of the thesis were that continuous filament fabrication was possible if CNF with anionic charge was in the core and cationic CNF was on the shell during coaxial spinning. When filaments were lifted to the winder, filament support, reduced friction and properly directed drying air were the key elements for successful filament fabrication. Additionally, air removal from CNFs was important to prevent filament from breaking.

Mechanical tests revealed that drying temperature, spinning speed, washing and especially stretching significantly affect filament mechanical properties. Drying temperature of 500 – 550 °C, 20 – 50 % higher spinning speed of shell, and larger needle were advantageous for filament properties. Additionally, stretching was shown to be important for better filament mechanical properties. At the highest, tensile strength and Young's modulus of 11 MPa and 787 MPa, respectively for TO-CNF/CDAC-CNF, and 7.1 MPa and 260 MPa, respectively for S-CNF/CDAC-CNF, were reached. Additionally, washing was shown to notable increase tensile strength of the filaments, thus washed filaments reached the highest tensile strengths; 67 MPa for TO-CNF/CDAC-CNF, 105 MPa for S-CNF/CDAC-CNF, and 78 MPa for TO-CNF/TO-CNF.

Compared to TO-CNF/TO-CNF, S-CNF/CDAC-CNF and TO-CNF/CDAC-CNF were not shown to have remarkable difference even if TO-CNF/TO-CNF had mostly higher level of tensile strength. On a large scale, tensile strength of all filaments was rather close to each other, with even highest tensile strength reached for washed S-CNF/CDAC-CNF.

Additionally, S-CNF/CDAC-CNF was purely based on DES CNF. Thus, greener core-shell filaments showed potential to be used in filament fabrication. However, mechanical properties were significantly lower compared to previously fabricated filaments by interfacial complexation and other spinning methods most probably due to poor CNF orientation and lacking of washing step. Thus, further research is needed for optimization of the continuous filament spinning process.

REFERENCES

Abbott, A.P., Barron, J.C., Ryder, K.S. & Wilson, D., 2007. Eutectic-based ionic liquids with metal-containing anions and cations. Chemistry - A European Journal, 13 (22), pp. 6495-6501.

Abbott, A.P., Capper, G., Davies, D.L., Rasheed, R.K. & Tambyrajah, V., 2003. Novel solvent properties of choline chloride/urea mixtures. Chemical Communications, 9 (1), pp. 70-71.

Agarwal, V., Huber, G.W., Conner Jr., W.C. & Auerbach, S.M., 2011. Simulating infrared spectra and hydrogen bonding in cellulose Iβ at elevated temperatures. Journal of Chemical Physics, 135 (13).

Ashworth, C.R., Matthews, R.P., Welton, T. & Hunt, P.A., 2016. Doubly ionic hydrogen bond interactions within the choline chloride-urea deep eutectic solvent. Physical Chemistry Chemical Physics, 18 (27), pp. 18145-18160.

Bordel, D., Putaux, J.-. & Heux, L., 2006. Orientation of native cellulose in an electric field. Langmuir, 22 (11), pp. 4899-4901.

Cai, Y., Geng, L., Chen, S., Shi, S., Hsiao, B.S. & Peng, X., 2020. Hierarchical Assembly of Nanocellulose into Filaments by Flow-Assisted Alignment and Interfacial Complexation: Conquering the Conflicts between Strength and Toughness. ACS Applied Materials and Interfaces, 12, (28), pp. 32090-32098.

Carriazo, D., Serrano, M.C., Gutiérrez, M.C., Ferrer, M.L. & del Monte, F., 2012. Deep-eutectic solvents playing multiple roles in the synthesis of polymers and related materials. Chemical Society Reviews, 41 (14), pp. 4996-5014.

Choi, Y.H., van Spronsen, J., Dai, Y., Verberne, M., Hollmann, F., Arends, I. W. C. E., Witkamp, G.-. & Verpoorte, R., 2011. Are natural deep eutectic solvents the missing link in understanding cellular metabolism and physiology?. Plant Physiology, 156 (4), pp. 1701-1705.

Christopher, L. P., 2012. Adding Value Prior to Pulping: Bioproducts from Hemicellulose. Global Perspectives on Sustainable Forest Management, Dr. Dr. Clement A. Okia (Ed.), ISBN: 978-953-51-0569-5.

Ciolacu, D. & Popa, V.I. 2010. Cellulose allomorphs - Overview and perspectives. In Cellulose: Structure and Properties, Derivatives and Industrial Uses Nova Science Publishers, Inc., pp. 1-38. ISBN 978-1-60876-388-7.

Cui, Q., Bell, D.J., Rauer, S.B. & Wessling, M., 2020. Wet-Spinning of Biocompatible Core–Shell Polyelectrolyte Complex Fibers for Tissue Engineering. Advanced Materials Interfaces, 7 (23).

Dai, Y., van Spronsen, J., Witkamp, G.-., Verpoorte, R. & Choi, Y.H., 2013. Natural deep eutectic solvents as new potential media for green technology. Analytica Chimica Acta, 766, pp. 61-68.

Dhali, K., Ghasemlou, M., Daver, F., Cass, P. & Adhikari, B., 2021. A review of nanocellulose as a new material towards environmental sustainability. Science of the Total Environment, 775.

Dhillon, G. S., Gassara, F., Brar, S. K. & Verma, M., 2012. Biotechnological applications of lignin: “Sustainable alternative to non-renewable materials”. In: Paterson, R.J. (ed.) Lignin: Properties and Applications in Biotechnology and Bioenergy. New York: Nova Science Publishers, Inc., pp. 1-3. ISBN 978-1-61122-907-3.

Dinwoodie, J. M., 1978. Wood: Nature's cellular polymeric composite. Physics in Technology, 9 (5), pp. 185.

Dufresne, A., 2018. Nanocellulose: from nature to high performance tailored materials. Vol. 2. Berlin: de Gruyter. pp. 634. ISBN 978-3-11-048041-2.

Dufresne, A., 2019. Nanocellulose Processing Properties and Potential Applications. Current Forestry Reports, 5, pp. 76-89.

Eichhorn, S.J., Dufresne, A., Aranguren, M., Marcovich, N.E., Capadona, J.R., Rowan, S.J., Weder, C., Thielemans, W., Roman, M., Renneckar, S., Gindl, W., Veigel, S., Keckes, J., Yano, H., Abe, K., Nogi, M., Nakagaito, A.N., Mangalam, A., Simonsen, J., Benight, A.S., Bismarck, A., Berglund, L.A. & Peijs, T., 2010. Review: Current international research into cellulose nanofibres and nanocomposites. Journal of Materials Science, 45 (1), pp. 1-33.

Ek, M., Gellerstedt, G. & Henriksson, G., 2009. Wood chemistry and wood biotechnology. Wood Chemistry and Wood Biotechnology. Walter de Gruyter GmbH and Co. KG, pp. 309. ISBN 978-3-11-021339-3.

Fahma, F., Lisdayana, N., Lovely, B., Febiyanti, I., Noviana, D., Sari, Y.W., Yunus, M., Kusumaatmaja, A., Mukti, R.R. & Kadja, G.T.M., 2020. Potential application of nanocellulose for filaments production: A review. Journal of Nanostructures, 10 (3), pp. 553-563.

Gargulak, J. D., Lebo, S. E. & McNally, T. J., 2015. Lignin. Kirk-Othemer Encyclopedia of Chemical Thecnology.

Ghasemi, S., Tajvidi, M., Bousfield, D.W., Gardner, D.J. & Gramlich, W.M., 2017. Dry-spun neat cellulose nanofibril filaments: Influence of drying temperature and nanofibril structure on filament properties. Polymers, 9 (9)g.

Ghasemi, S., Tajvidi, M., Gardner, D.J., Bousfield, D.W. & Shaler, S.M., 2018. Effect of wettability and surface free energy of collection substrates on the structure and morphology of dry-spun cellulose nanofibril filaments. Cellulose, 25 (11), pp. 6305-6317.

Grande, R., Trovatti, E., Carvalho, A.J.F. & Gandini, A., 2017. Continuous microfiber drawing by interfacial charge complexation between anionic cellulose nanofibers and cationic chitosan. Journal of Materials Chemistry A, 5 (25), pp. 13098-13103.

Habibi, Y., 2014. Key advances in the chemical modification of nanocelluloses. Chemical Society Reviews, 43 (5), pp. 1519-1542.

Henriksson, M., Henriksson, G., Berglund, L. A., & Lindström, T., 2007. An environmentally friendly method for enzyme-assisted preparation of microfibrillated cellulose (MFC) nanofibers. European Polymer Journal, 43 (8), pp. 3434-3441.

Håkansson, K.M.O., Fall, A.B., Lundell, F., Yu, S., Krywka, C., Roth, S.V., Santoro, G., Kvick, M., Prahl Wittberg, L., Wågberg, L. & Söderberg, L.D., 2014. Hydrodynamic alignment and assembly of nanofibrils resulting in strong cellulose filaments. Nature Communications, 5 (1).

Ingrao, C., Bacenetti, J., Bezame, A., Blok, V., Geldermann, J., Goglio, P., Koukios, E.G., Lindner, M., Nemecek, T., Siracusa, V., Zabaniotou, A. and Huisingh, D., 2016. Agricultural and Forest Biomass for Food, Materials and Energy: Bio-Economy as the Cornerstone to Cleaner Production and More Sustainable Consumption Patterns for Accelerating the Transition towards Equitable, Sustainable, Post Fossil-Carbon Societies. Journal of Cleaner Production, 117, pp. 4-6.

Iwamoto, S., Isogai, A. & Iwata, T., 2011. Structure and mechanical properties of wet-spun fibers made from natural cellulose nanofibers. Biomacromolecules, 12 (3), pp. 831-836.

Jiang, F., Li, T., Li, Y., Zhang, Y., Gong, A., Dai, J., Hitz, E., Luo, W. & Hu, L., 2018. Wood-Based Nanotechnologies toward Sustainability. Advanced Materials, 30 (1).

Kafy, A., Kim, H.C., Zhai, L., Kim, J.W., Hai, L.V., Kang, T.J. & Kim, J., 2017. Cellulose long fibers fabricated from cellulose nanofibers and its strong and tough characteristics. Scientific Reports, 7 (1).

Kangas, H., 2014. Opas selluloosananomateriaaleihin [online document]. VTT. Available:https://www.vttresearch.com/sites/default/files/pdf/technology/2014/T199.pdf [referred 31.3.2021]. 97 s. ISBN 978-951-8194-8.

Kekäläinen, K., 2016. Microfibrillation of pulp fibres – The effects of compression-shearing, oxidation and thermal drying [online document]. Oulu: University of Oulu, Faculty of technology. pp. 114.

Kim, H.C., Kim, D., Lee, J.Y., Zhai, L. & Kim, J., 2019. Effect of Wet Spinning and Stretching to Enhance Mechanical Properties of Cellulose Nanofiber Filament. International Journal of Precision Engineering and Manufacturing - Green Technology, 6 (3), pp. 567-575.

Klemm, D., Heublein, B., Fink, H.-. & Bohn, A., 2005. Cellulose: Fascinating biopolymer and sustainable raw material. Angewandte Chemie - International Edition, 44 (22), pp. 3358-3393.

Klemm, D., Kramer, F., Moritz, S., Lindström, T., Ankerfors, M., Gray, D. & Dorris, A., 2011. Nanocelluloses: A new family of nature-based materials. Angewandte Chemie - International Edition, 50 (24), pp. 5438-5466.

Kumar, B., Bhardwaj, N., Agrawal, K., Chaturvedi, V. & Verma, P., 2020. Current perspective on pretreatment technologies using lignocellulosic biomass: An emerging biorefinery concept. Fuel Processing Technology, 199.

Li, P., Sirviö, J.A., Asante, B. & Liimatainen, H., 2018. Recyclable deep eutectic solvent for the production of cationic nanocelluloses. Carbohydrate Polymers, 199, pp. 219-227.

Liimatainen, H., Visanko, M., Sirviö, J.A., Hormi, O.E.O. & Niinimaki, J., 2012. Enhancement of the nanofibrillation of wood cellulose through sequential periodate-chlorite oxidation. Biomacromolecules, 13 (5), pp. 1592-1597.

Liimatainen, H., Visanko, M., Sirviö, J., Hormi, O. & Niinimäki, J., 2013. Sulfonated cellulose nanofibrils obtained from wood pulp through regioselective oxidative bisulfite pre-treatment. Cellulose, 20 (2), pp. 741-749.

Lindström, T., 2017. Aspects on nanofibrillated cellulose (NFC) processing, rheology and NFC-film properties. Current Opinion in Colloid and Interface Science, 29, pp. 68-75.

Lundahl, M.J., Cunha, A.G., Rojo, E., Papageorgiou, A.C., Rautkari, L., Arboleda, J.C. & Rojas, O.J., 2016. Strength and Water Interactions of Cellulose i Filaments Wet-Spun from Cellulose Nanofibril Hydrogels. Scientific Reports, 6.

Lundahl, M.J., Klar, V., Ajdary, R., Norberg, N., Ago, M., Cunha, A.G. & Rojas, O.J., 2018. Absorbent Filaments from Cellulose Nanofibril Hydrogels through Continuous Coaxial Wet Spinning. ACS Applied Materials and Interfaces, 10 (32), pp. 27287-27296.

Lundahl, M.J., Berta, M., Ago, M., Stading, M. & Rojas, O.J., 2018b. Shear and extensional rheology of aqueous suspensions of cellulose nanofibrils for biopolymer-assisted filament spinning. European Polymer Journal, 109, pp. 367-378.

Lundahl, M.J., Klar, V., Wang, L., Ago, M. & Rojas, O.J., 2017. Spinning of cellulose nanofibrils into filaments: A review. Industrial and Engineering Chemistry Research, 56 (1), pp. 8-19.

Marais, A., Erlandsson, J., Söderberg, L. D., & Wågberg, L., 2020. Coaxial Spinning of Oriented Nanocellulose Filaments and Core–Shell Structures for Interactive Materials and Fiber-Reinforced Composites. ACS Applied Nano Materials, 3 (10), pp. 10246-10251.

Mendoza, L., Gunawardhana, T., Batchelor, W. & Garnier, G. 2018. Effects of fibre dimension and charge density on nanocellulose gels. Journal of colloid and interface science, 525, pp. 119-125.

Mertaniemi, H., Escobedo-Lucea, C., Sanz-Garcia, A., Gandía, C., Mäkitie, A., Partanen, J., Ikkala, O. & Yliperttula, M., 2016. Human stem cell decorated nanocellulose threads for biomedical applications. Biomaterials, 82, pp. 208-220.

Michud, A., Hummel, M. & Sixta, H., 2015. Influence of molar mass distribution on the final properties of fibers regenerated from cellulose dissolved in ionic liquid by dry-jet wet spinning. Polymer, 75, pp. 1-9.

Mittal, N., Ansari, F., Gowda Krishne, V., Brouzet, C., Chen, P., Larsson, P.T., Roth, S.V., Lundell, F., Wågberg, L., Kotov, N.A. & Söderberg, L.D., 2018. Multiscale Control of Nanocellulose Assembly: Transferring Remarkable Nanoscale Fibril Mechanics to Macroscale Fibers. ACS Nano, 12 (7), pp. 6378-6388.

Naderi, A., Lindström, T. & Sundström, J., 2015. Repeated homogenization, a route for decreasing the energy consumption in the manufacturing process of carboxymethylated nanofibrillated cellulose? Cellulose, 22 (2), pp. 1147-1157.

Nechyporchuk, O., Belgacem, M.N. & Bras, J., 2016. Production of cellulose nanofibrils: A review of recent advances. Industrial Crops and Products, 93, pp. 2-25.

Nechyporchuk, O., Håkansson, K.M.O., Gowda.V, K., Lundell, F., Hagström, B. & Köhnke, T., 2019. Continuous Assembly of Cellulose Nanofibrils and Nanocrystals into Strong Macrofibers through Microfluidic Spinning. Advanced Materials Technologies, 4 (2).

Olszewska, A., Eronen, P., Johansson, L.-., Malho, J.-., Ankerfors, M., Lindström, T., Ruokolainen, J., Laine, J. & Österberg, M., 2011. The behaviour of cationic NanoFibrillar Cellulose in aqueous media. Cellulose, 18 (5), pp. 1213-1226.

Peng, Y., Gardner, D.J. & Han, Y., 2012. Drying cellulose nanofibrils: In search of a suitable method. Cellulose, 19 (1), pp. 91-102.

Pullawan, T., Wilkinson, A.N. & Eichhorn, S.J., 2012. Influence of magnetic field alignment of cellulose whiskers on the mechanics of all-cellulose nanocomposites. Biomacromolecules, 13 (8), pp. 2528-2536.

Pääkko, M., Ankerfors, M., Kosonen, H., Nykänen, A., Ahola, S., Österberg, M., Ruokolainen, J., Laine, J., Larsson, P.T., Ikkala, O. & Lindström, T., 2007. Enzymatic hydrolysis combined with mechanical shearing and high-pressure homogenization for nanoscale cellulose fibrils and strong gels. Biomacromolecules, 8 (6), pp. 1934-1941.

Rosén, T., Hsiao, B.S. & Söderberg, L.D., 2020. Elucidating the Opportunities and Challenges for Nanocellulose Spinning. Advanced Materials.

Rosén, T., Mittal, N., Roth, S.V., Zhang, P., Lundell, F. & Söderberg, L.D., 2020b. Flow fields control nanostructural organization in semiflexible networks. Soft Matter, 16 (23) pp. 5439-5449.

Selkälä, T., Sirviö, J.A., Lorite, G.S. & Liimatainen, H., 2016. Anionically Stabilized Cellulose Nanofibrils through Succinylation Pretreatment in Urea–Lithium Chloride Deep Eutectic Solvent. ChemSusChem, 9 (21), pp. 3074-3083.

Siró, I. & Plackett, D., 2010. Microfibrillated cellulose and new nanocomposite materials: A review. Cellulose, 17 (3), pp. 459-494.

Sirviö, J.A., 2018. Cationization of lignocellulosic fibers with betaine in deep eutectic solvent: Facile route to charge stabilized cellulose and wood nanofibers. Carbohydrate Polymers, 198, pp. 34-40.

Sirviö, J.A., Ukkola, J. & Liimatainen, H., 2019. Direct sulfation of cellulose fibers using a reactive deep eutectic solvent to produce highly charged cellulose nanofibers. Cellulose, 26 (4), pp. 2303-2316.

Sirviö, J.A. & Visanko, M., 2017. Anionic wood nanofibers produced from unbleached mechanical pulp by highly efficient chemical modification. Journal of Materials Chemistry A, 5 (41), pp. 21828-21835.

Sirviö, J.A., Visanko, M. & Liimatainen, H., 2015. Deep eutectic solvent system based on choline chloride-urea as a pre-treatment for nanofibrillation of wood cellulose. Green Chemistry, 17 (6), pp. 3401-3406.

Smith, E. L., Abbott, A. P., & Ryder, K. S., 2014. Deep eutectic solvents (DESs) and their applications. Chemical reviews, 114 (21), pp. 11060-11082.

Stefanovic, R., Ludwig, M., Webber, G.B., Atkin, R. & Page, A.J., 2017. Nanostructure, hydrogen bonding and rheology in choline chloride deep eutectic solvents as a function of the hydrogen bond donor. Physical Chemistry Chemical Physics, 19 (4), pp. 3297-3306.

Stelte, W., & Sanadi, A. R., 2009. Preparation and characterization of cellulose nanofibers from two commercial hardwood and softwood pulps. Industrial & engineering chemistry research, 48 (24), pp. 11211-11219.

Stenius, P. 2000. Papermaking science and technology: Book 3, Forest products chemistry. Jyväskylä: Fapet Oy. pp.350. ISBN 952-5216-03-9.

Tenhunen, T.-., Lewandowska, A.E., Orelma, H., Johansson, L.-., Virtanen, T., Harlin, A., Österberg, M., Eichhorn, S.J. & Tammelin, T., 2018. Understanding the interactions of cellulose fibres and deep eutectic solvent of choline chloride and urea. Cellulose, 25 (1), pp. 137-150.

Tingaut, P., Zimmermann, T. & Sèbe, G., 2012. Cellulose nanocrystals and microfibrillated cellulose as building blocks for the design of hierarchical functional materials. Journal of Materials Chemistry, 22 (38), pp. 20105-20111.

Torres-Rendon, J.G., Schacher, F.H., Ifuku, S. & Walther, A., 2014. Mechanical performance of macrofibers of cellulose and chitin nanofibrils aligned by wet-stretching: A critical comparison. Biomacromolecules, 15 (7), pp. 2709-2717.

Vuoriluoto, M., Orelma, H., Lundahl, M., Borghei, M. & Rojas, O.J., 2017. Filaments with Affinity Binding and Wet Strength Can Be Achieved by Spinning Bifunctional Cellulose Nanofibrils Biomacromolecules, 18 (6), pp. 1803-1813.

Wang, L., Lundahl, M.J., Greca, L.G., Papageorgiou, A.C., Borghei, M. & Rojas, O.J., 2019. Effects of non-solvents and electrolytes on the formation and properties of cellulose I filaments. Scientific Reports, 9 (1).

Woodings, C., 2001. A brief history of regenerated cellulose fibres, in Woodings, C. (Ed.) Regenerated Cellulose Fibres. Woodhead Publishing Limited, Boca Raton, FL. pp. 1–21.

Wågberg, L., Decher, G., Norgren, M., Lindström, T., Ankerfors, M. & Axnäs, K., 2008. The build-up of polyelectrolyte multilayers of microfibrillated cellulose and cationic polyelectrolytes. Langmuir, 24 (3), pp. 784-795.

Zahn, S., Kirchner, B. & Mollenhauer, D., 2016. Charge Spreading in Deep Eutectic Solvents. ChemPhysChem, 17 (21), pp. 3354-3358.

Zhang, K., Ketterle, L., Järvinen, T., Hong, S. & Liimatainen, H., 2020b. Conductive hybrid filaments of carbon nanotubes, chitin nanocrystals and cellulose nanofibers formed by interfacial nanoparticle complexation. Materials and Design, 191.

Zhang, K., Ketterle, L., Järvinen, T., Lorite, G.S., Hong, S. & Liimatainen, H., 2020a. Self-assembly of graphene oxide and cellulose nanocrystals into continuous filament via interfacial nanoparticle complexation. Materials and Design, 193.

Zhang, K. & Liimatainen, H., 2018. Hierarchical Assembly of Nanocellulose-Based Filaments by Interfacial Complexation. Small, 14 (38).

Zhang, L., Mao, Y., Zhou, J. & Cai, J. 2005. Effects of coagulation conditions on the properties of regenerated cellulose films prepared in NaOH/Urea aqueous solution. Industrial and Engineering Chemistry Research, 44 (3), pp. 522-529.

Zhang, Q., De Oliveira Vigier, K., Royer, S. & Jérôme, F., 2012. Deep eutectic solvents: Syntheses, properties and applications. Chemical Society Reviews, 41 (21), pp. 7108-71

APPENDIXES

APPENDIX 1. Table of fabricated filaments

APPENDIX 2. Table of fabricated filaments and their corresponding mechanical properties in terms of tensile strength, Young's modulus and strain at tensile strength, and width.

APPENDIX 3. Figure of washed filament

APPENDIX 1. Table of fabricated filaments.

Table 2. Fabricated filaments.

Filament	Needle	Filament composition		Spinning speed (mL/min)		Drawing speed		Drying temperature (°C)	Washing
		core	shell	core	shell	Winder	cm/min		
TO-CNF1.8%/CDAC-CNF1.9%_0.350_W4_650	20G/16G	TO-CNF	CDAC-CNF	0.350	0.350	W4	126	650	No
TO-CNF1.8%/CDAC-CNF1.9%_0.350_W4_600	20G/16G	TO-CNF	CDAC-CNF	0.350	0.350	W4	126	600	No
TO-CNF1.8%/CDAC-CNF1.9%_0.350_W4_550	20G/16G	TO-CNF	CDAC-CNF	0.350	0.350	W4	126	550	No
TO-CNF1.8%/CDAC-CNF1.9%_0.350_W4_500	20G/16G	TO-CNF	CDAC-CNF	0.350	0.350	W4	126	500	No
TO-CNF1.8%/CDAC-CNF1.9%_0.350_W4_450	20G/16G	TO-CNF	CDAC-CNF	0.350	0.350	W4	126	450	No
TO-CNF1.8%/CDAC-CNF1.9%_0.250_W3_650	20G/16G	TO-CNF	CDAC-CNF	0.250	0.250	W3	94	650	No
TO-CNF1.8%/CDAC-CNF1.9%_0.450_W4_650	20G/16G	TO-CNF	CDAC-CNF	0.450	0.450	W4	126	650	No
TO-CNF1.8%/CDAC-CNF1.9%_0.550_W6_650	20G/16G	TO-CNF	CDAC-CNF	0.550	0.550	W6	188	650	No
TO-CNF1.8%/CDAC-CNF1.9%_0.550_UST_650	20G/16G	TO-CNF	CDAC-CNF	0.550	0.550	UST	-	650	No
TO-CNF1.8%/CDAC-CNF1.9%_0.350/0.450_W4_650	20G/16G	TO-CNF	CDAC-CNF	0.350	0.450	W4	126	650	No
TO-CNF1.8%/CDAC-CNF1.9%_0.350/0.550_W4_650	20G/16G	TO-CNF	CDAC-CNF	0.350	0.550	W4	126	650	No
TO-CNF1.8%/CDAC-CNF1.9%_0.350/0.650_W4_650	20G/16G	TO-CNF	CDAC-CNF	0.350	0.650	W4	126	650	No
S-CNF1.6%/CDAC-CNF1.6%_0.350_W3_650	20G/16G	S-CNF	CDAC-CNF	0.350	0.350	W3	94	650	No
S-CNF1.6%/CDAC-CNF1.6%_0.350_W3_600	20G/16G	S-CNF	CDAC-CNF	0.350	0.350	W3	94	600	No
S-CNF1.6%/CDAC-CNF1.6%_0.350_W3_550	20G/16G	S-CNF	CDAC-CNF	0.350	0.350	W3	94	550	No
S-CNF1.6%/CDAC-CNF1.6%_0.350_W3_500	20G/16G	S-CNF	CDAC-CNF	0.350	0.350	W3	94	500	No
S-CNF1.6%/CDAC-CNF1.6%_0.350_W3_450	20G/16G	S-CNF	CDAC-CNF	0.350	0.350	W3	94	450	No
S-CNF1.6%/CDAC-CNF1.6%_0.250_W2_650	20G/16G	S-CNF	CDAC-CNF	0.250	0.250	W2	63	650	No
S-CNF1.6%/CDAC-CNF1.6%_0.450_W3_650	20G/16G	S-CNF	CDAC-CNF	0.450	0.450	W3	94	650	No
S-CNF1.6%/CDAC-CNF1.6%_0.550_W4_650	20G/16G	S-CNF	CDAC-CNF	0.550	0.550	W4	126	650	No
S-CNF1.6%/CDAC-CNF1.6%_0.450/0.550_W3_650	20G/16G	S-CNF	CDAC-CNF	0.450	0.550	W3	94	650	No
S-CNF1.6%/CDAC-CNF1.6%_0.450/0.650_W3_650	20G/16G	S-CNF	CDAC-CNF	0.450	0.650	W3	94	650	No
S-CNF1.6%/CDAC-CNF1.6%_0.450/0.750_W3_650	20G/16G	S-CNF	CDAC-CNF	0.450	0.750	W3	94	650	No
TO-CNF1.8%/TO-CNF1.8%_0.350_W2_650	20G/16G	TO-CNF	TO-CNF	0.350	0.350	W2	63	650	No
TO-CNF1.8%/TO-CNF1.8%_0.350_W2_600	20G/16G	TO-CNF	TO-CNF	0.350	0.350	W2	63	600	No
TO-CNF1.8%/TO-CNF1.8%_0.350_W2_550	20G/16G	TO-CNF	TO-CNF	0.350	0.350	W2	63	550	No
TO-CNF1.8%/TO-CNF1.8%_0.350_W2_500	20G/16G	TO-CNF	TO-CNF	0.350	0.350	W2	63	500	No
TO-CNF1.8%/TO-CNF1.8%_0.350_W2_450	20G/16G	TO-CNF	TO-CNF	0.350	0.350	W2	63	450	No
TO-CNF1.8%/TO-CNF1.8%_0.250_W2_650	20G/16G	TO-CNF	TO-CNF	0.250	0.250	W2	63	650	No
TO-CNF1.8%/TO-CNF1.8%_0.450_W3_650	20G/16G	TO-CNF	TO-CNF	0.450	0.450	W3	94	650	No
TO-CNF1.8%/TO-CNF1.8%_0.550_W3_650	20G/16G	TO-CNF	TO-CNF	0.550	0.550	W3	94	650	No
TO-CNF1.8%/TO-CNF1.8%_0.350/0.450_W3_650	20G/16G	TO-CNF	TO-CNF	0.350	0.450	W3	94	650	No
TO-CNF1.8%/TO-CNF1.8%_0.350/0.550_W3_650	20G/16G	TO-CNF	TO-CNF	0.350	0.550	W3	94	650	No
TO-CNF1.8%/TO-CNF1.8%_0.350/0.650_W3_650	20G/16G	TO-CNF	TO-CNF	0.350	0.650	W3	94	650	No
22G/18G_TO-CNF1.8%/CDAC-CNF1.9%_0.350/0.350_W6_500	22G/18G	TO-CNF	CDAC-CNF	0.350	0.350	W6	188	500	No
22G/18G_TO-CNF1.8%/CDAC-CNF1.9%_0.350/0.450_W6_500	22G/18G	TO-CNF	CDAC-CNF	0.350	0.450	W6	188	500	No
22G/18G_TO-CNF1.8%/CDAC-CNF1.9%_0.350/0.550_W6_500	22G/18G	TO-CNF	CDAC-CNF	0.350	0.550	W6	188	500	No
22G/18G_TO-CNF1.8%/CDAC-CNF1.9%_0.350/0.650_W8_500	22G/18G	TO-CNF	CDAC-CNF	0.350	0.650	W8	269	500	No
22G/18G_S-CNF1.6%/CDAC-CNF1.6%_0.450/0.450_W4_500	22G/18G	S-CNF	CDAC-CNF	0.450	0.450	W4	126	500	No
22G/18G_S-CNF1.6%/CDAC-CNF1.6%_0.450/0.550_W4_500	22G/18G	S-CNF	CDAC-CNF	0.450	0.550	W5	157	500	No
22G/18G_S-CNF1.6%/CDAC-CNF1.6%_0.450/0.650_W6_500	22G/18G	S-CNF	CDAC-CNF	0.450	0.650	W6	188	500	No
22G/18G_S-CNF1.6%/CDAC-CNF1.6%_0.450/0.750_W6_500	22G/18G	S-CNF	CDAC-CNF	0.450	0.750	W6	188	500	No
Washed_S-CNF1.6%/CDAC-CNF1.6% 0.450/0.550_W3_650	20G/16G	S-CNF	CDAC-CNF	0.450	0.550	W3	94	650	Yes
Washed_TO-CNF1.8%/CDAC-CNF1.9% 0.350/0.450_W4_650	20G/16G	TO-CNF	CDAC-CNF	0.350	0.450	W4	126	650	Yes
Washed_TO-CNF1.8%/TO-CNF1.8% 0.350/0.450_W3_650	20G/16G	TO-CNF	TO-CNF	0.350	0.450	W3	94	650	Yes

APPENDIX 2. Table of fabricated filaments and their corresponding mechanical properties in terms of tensile strength, Young's modulus and strain at tensile strength, and width.

Table 3. Fabricated filaments and their corresponding mechanical properties in terms of tensile strength, Young's modulus and strain at tensile strength, and width.

Filament	Tensile strength (MPa)	Young's modulus (MPa)	Strain at tensile strength (%)	Width (µm)	Drawing ratio
TO-CNF1.8%/CDAC-CNF1.9%_0.350_W4_650	4.6 ± 0.4	338 ± 59	1.9 ± 0.2	199 ± 38	0,96
TO-CNF1.8%/CDAC-CNF1.9%_0.350_W4_600	7.3 ± 1.7	438 ± 176	2.1 ± 0.2	132 ± 14	0,96
TO-CNF1.8%/CDAC-CNF1.9%_0.350_W4_550	7.2 ± 0.4	563 ± 56	1.9 ± 0.2	152 ± 17	0,96
TO-CNF1.8%/CDAC-CNF1.9%_0.350_W4_500	8.2 ± 1	577 ± 93	2.4 ± 0.2	137 ± 29	0,96
TO-CNF1.8%/CDAC-CNF1.9%_0.350_W4_450	5.3 ± 0.6	341 ± 75	1.9 ± 0.1	163 ±11	0,96
TO-CNF1.8%/CDAC-CNF1.9%_0.250_W3_650	4.6 ± 0.2	220 ± 8.9	2.5 ± 0.2	207 ± 46	1,01
TO-CNF1.8%/CDAC-CNF1.9%_0.450_W4_650	5.9 ± 0.6	443 ± 60	2.0 ± 0.4	170 ± 9	0,75
TO-CNF1.8%/CDAC-CNF1.9%_0.550_W6_650	11 ± 0.6	786 ± 105	2.4 ± 0.2	141 ± 10	0,92
TO-CNF1.8%/CDAC-CNF1.9%_0.550_UST_650	5.2 ± 0.3	321 ± 26	2.2 ± 0.2	213 ± 25	0,00
TO-CNF1.8%/CDAC-CNF1.9%_0.350/0.450_W4_650	8.2 ± 0.3	676 ± 61	1.7 ± 0.1	158 ± 15	0,75
TO-CNF1.8%/CDAC-CNF1.9%_0.350/0.550_W4_650	8.0 ± 0.3	648 ± 48	2.0 ±0.2	159 ± 10	0,61
TO-CNF1.8%/CDAC-CNF1.9%_0.350/0.650_W4_650	5.1 ± 0.1	333 ± 52	2.2 ± 0.1	191 ± 25	0,52
S-CNF1.6%/CDAC-CNF1.6%_0.350_W3_650	5.7 ± 0.5	213 ± 32	3.5 ± 0.5	162 ± 21	0,72
S-CNF1.6%/CDAC-CNF1.6%_0.350_W3_600	5.9 ± 0.5	206 ± 19	4.2 ± 0.2	165 ± 16	0,72
S-CNF1.6%/CDAC-CNF1.6%_0.350_W3_550	7.0 ± 0.3	259 ± 16	4.1 ± 0.3	139 ± 16	0,72
S-CNF1.6%/CDAC-CNF1.6%_0.350_W3_500	5.8 ± 0.6	224 ± 43	3.5 ± 0.4	151 ± 13	0,72
S-CNF1.6%/CDAC-CNF1.6%_0.350_W3_450	5.3 ± 0.4	181 ± 22	3.8 ± 0.3	161 ± 17	0,72
S-CNF1.6%/CDAC-CNF1.6%_0.250_W2_650	2.6 ± 0.1	19 ± 6.0	20 ± 1.1	258 ± 56	0,68
S-CNF1.6%/CDAC-CNF1.6%_0.450_W3_650	2.7 ± 0.2	33 ± 4.2	19 ± 2.2	265 ± 29	0,56
S-CNF1.6%/CDAC-CNF1.6%_0.550_W4_650	3.3 ± 0.4	44 ± 6.4	20 ± 2.8	210 ± 33	0,61
S-CNF1.6%/CDAC-CNF1.6%_0.450/0.550_W3_650	6.0 ± 0.4	77 ± 4.4	24 ± 1.8	181 ± 22	0,46
S-CNF1.6%/CDAC-CNF1.6%_0.450/0.650_W3_650	6.3 ± 0.7	70 ± 10	19 ± 1.9	172 ± 17	0,39
S-CNF1.6%/CDAC-CNF1.6%_0.450/0.750_W3_650	3.4 ± 0.3	42 ± 10	18 ± 3.5	217 ± 17	0,34
TO-CNF1.8%/TO-CNF1.8%_0.350_W2_650	7.5 ± 0.8	153 ± 45	7.6 ± 1.0	230 ± 31	0,48
TO-CNF1.8%/TO-CNF1.8%_0.350_W2_600	8.8 ± 0.5	71 ± 37	16 ± 1.4	235 ± 20	0,48
TO-CNF1.8%/TO-CNF1.8%_0.350_W2_550	6.4 ± 0.8	81 ± 4.1	17 ± 6.9	254 ± 19	0,48
TO-CNF1.8%/TO-CNF1.8%_0.350_W2_500	13 ± 1.2	64 ± 38	21 ± 2.5	224 ± 25	0,48
TO-CNF1.8%/TO-CNF1.8%_0.350_W2_450	7.5 ± 0.4	19 ± 3.5	21 ± 0.8	275 ± 14	0,48
TO-CNF1.8%/TO-CNF1.8%_0.250_W2_650	6.0 ± 0.3	24 ± 13	20 ± 0.8	309 ± 24	0,68
TO-CNF1.8%/TO-CNF1.8%_0.450_W3_650	18 ± 1.3	12 ± 5.0	19 ± 1.9	219 ± 25	0,56
TO-CNF1.8%/TO-CNF1.8%_0.550_W3_650	15 ± 1.0	19 ± 10	18 ± 2.0	258 ± 19	0,46
TO-CNF1.8%/TO-CNF1.8%_0.350/0.450_W3_650	16 ± 1.9	55 ± 18	10 ± 1.8	186 ± 15	0,56
TO-CNF1.8%/TO-CNF1.8%_0.350/0.550_W3_650	22 ± 3.4	26 ± 4.4	17 ± 3.5	213 ± 18	0,46
TO-CNF1.8%/TO-CNF1.8%_0.350/0.650_W3_650	26 ± 0.8	44 ± 22	18 ± 1.4	183 ± 17	0,39
22G/18G_TO-CNF1.8%/CDAC-CNF1.9%_0.350/0.350_W6_500	4.6 ± 0.1	155 ± 23	11 ± 1.5	153 ± 67	0,70
22G/18G_TO-CNF1.8%/CDAC-CNF1.9%_0.350/0.450_W6_500	4.5 ± 0.1	147 ± 8.0	12 ± 0.3	153 ± 26	0,54
22G/18G_TO-CNF1.8%/CDAC-CNF1.9%_0.350/0.550_W6_500	3.6 ± 0.1	150 ± 12	8.7 ± 1.4	164 ± 17	0,44
22G/18G_TO-CNF1.8%/CDAC-CNF1.9%_0.350/0.650_W8_500	4.3 ± 0.3	189 ± 36	7.8 ± 0.5	153 ± 23	0,54
22G/18G_S-CNF1.6%/CDAC-CNF1.6%_0.450/0.450_W4_500	2.6 ± 0.2	56 ± 10	22 ± 1.0	245 ± 16	0,36
22G/18G_S-CNF1.6%/CDAC-CNF1.6%_0.450/0.550_W4_500	4.0 ± 0.3	100 ± 11	19 ± 3.1	200 ± 16	0,37
22G/18G_S-CNF1.6%/CDAC-CNF1.6%_0.450/0.650_W6_500	2.9 ± 0.1	80 ± 9.0	20 ± 1.2	202 ± 15	0,37
22G/18G_S-CNF1.6%/CDAC-CNF1.6%_0.450/0.750_W6_500	4.9 ± 0.3	120 ± 32	21 ± 1.6	161 ± 20	0,32
Washed_S-CNF1.6%/CDAC-CNF1.6% 0.450/0.550_W3_650	105 ± 18	51 ± 36	11 ± 4.0	152 ± 17	0,46
Washed_TO-CNF1.8%/CDAC-CNF1.9% 0.350/0.450_W4_650	67 ± 33	116 ± 99	4.5 ± 2.1	139 ± 21	0,75
Washed_TO-CNF1.8%/TO-CNF1.8% 0.350/0.450_W3_650	78 ± 4.5	21 ± 11	8.7 ± 1.9	200 ± 21	0,56

APPENDIX 3. Images of washed filament.

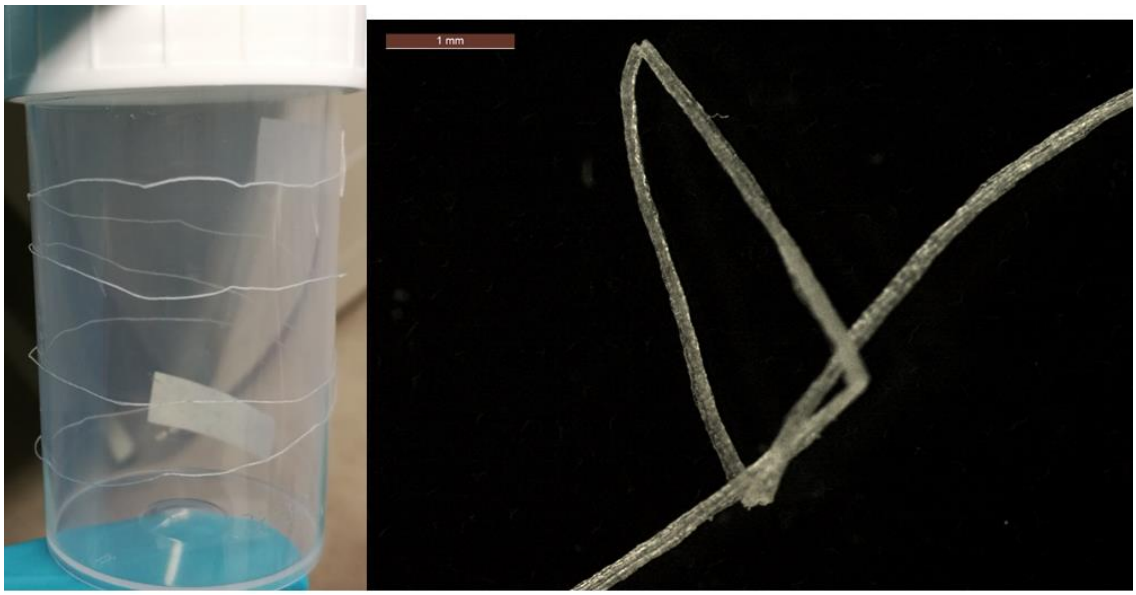

Figure 26. Washed filament.